Bringing service to life

ConnectFlow Verification
Release 9.6

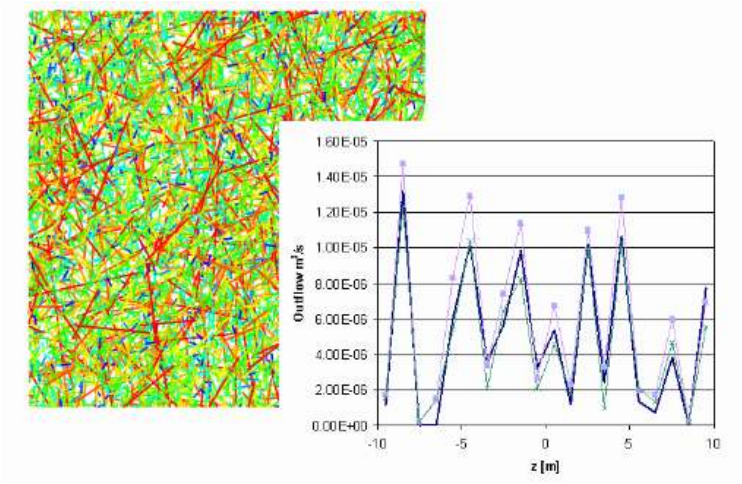

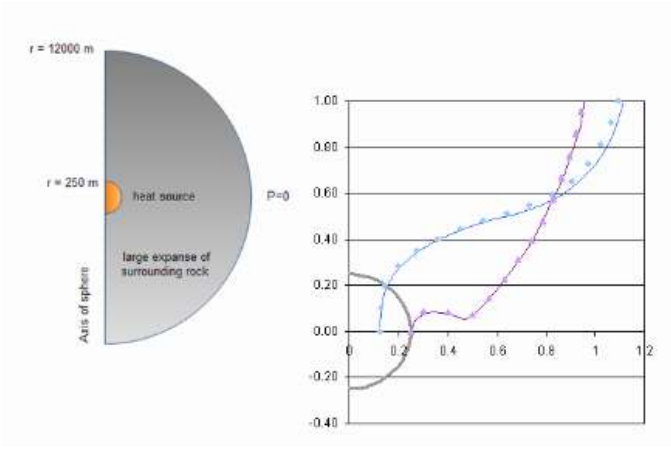

Prepared for

Prepared by Serco

Your Reference

Our Reference SA/ENV/CONNECTFLOW/16

Classification SERCO PUBLIC

Design | Advise | Integrate | Deliver

Title	ConnectFlow Verification Release 9.6
Prepared for	
Your Reference	
Our Reference	SA/ENV/CONNECTFLOW/16
Confidentiality, copyright & reproduction	SERCO PUBLIC This report is submitted by Serco Technical Consulting Services (hereafter referred to as Serco) in connection with a contract to supply goods and/or services and is submitted only on the basis of strict confidentiality. The contents must not be disclosed to third parties other than in accordance with the terms of the contract.
Contact Details	Technical & Assurance Services Building 150 Harwell IBC Didcot Oxfordshire OX11 0QB Telephone: 01635 280300 Facsimile: 01635 280305 Email: gw.support@serco.com Technical & Assurance Services is part of Serco Defence, Science and Technology, a division of Serco Ltd. In the areas where this work was performed, Technical & Assurance Services is certified to ISO 9001 (2000) and ISO 14001.

Executive Summary

ConnectFlow is the suite of Serco's groundwater modelling software that combines the NAMMU continuum porous medium (CPM) module and the NAPSAC discrete fracture network (DFN) module. ConnectFlow can be used very flexibly to model groundwater flow and transport in both fractured and porous media on a variety of scales.

The following documentation is available for ConnectFlow:

- ConnectFlow Technical Summary Document;
- ConnectFlow Command Reference Manual;
- ConnectFlow Verification Document;
- ConnectFlow Installation and Running Guide.

The following documentation is available for NAMMU:

- NAMMU Technical Summary Document;
- NAMMU User Guide;
- NAMMU Command Reference Manual;
- NAMMU Installation and Running Guide.

The following documentation is available for NAPSAC:

- NAPSAC Technical Summary Document;
- NAPSAC On-line Help;
- NAPSAC Installation and Running Guide.

This document, the Verification Document, provides information on the verification of ConnectFlow, which builds confidence in its flow and transport models.

Contents

1 Introduction

ConnectFlow is the suite of Serco's groundwater modelling software that combines the NAMMU continuum porous medium (CPM) module and the NAPSAC discrete fracture network (DFN) module. ConnectFlow can be used very flexibly to model groundwater flow and transport in both fractured and porous media on a variety of scales.

ConnectFlow models have been used in the following applications:

- safety assessment calculation in support of radioactive waste disposal programmes;
- modelling in support of groundwater protection schemes;
- modelling of landfills;
- regional groundwater flow;
- aquifer contamination;
- site investigation;
- pump test simulation;
- tracer tests;
- saline intrusion;
- design and evaluation of remediation strategies.

Further details of the ConnectFlow's capabilities can be found in [1] and [2].

The ConnectFlow software has been developed over a period of more than 20 years under a rigorous quality system that conforms to the international standards ISO 9001 and TickIT.

The purpose of this document is to present evidence that ConnectFlow is an appropriate tool to use for modelling groundwater flow and transport. This evidence takes the form of

- Comparison with analytical solutions.
- Comparison of results against other independently written groundwater flow software.

Sections 2, 3 and 4 provide details of a set of verification test cases and associated results. In all cases the results are considered "good" in terms of agreement with the reference data.

A number of the test cases are re-used to extend the range of capabilities tested. These variations include boundary condition types, mesh topology and algorithmic choices.

Section 5 references further testing that has taken place on the ConnectFlow suite of software, which complements and extends the testing covered in the earlier sections.

2 Continuum Porous Media Verification

A summary of the CPM test cases is given in Table 2-1.

Case	Title	Overview
2.1	Radial steady state flow.	Steady state groundwater flow. Modelled using hexahedral, prismatic and constrained meshes. Boundary conditions include mass flux, constant pressure and point sinks.
2.2	Steady state flow in fractured rock.	Steady state groundwater flow. Variations include mesh aligned with fractures and a regular mesh with permeabilties modified via an imported fracture file.
2.3	2D Steady state flow with particle tracks.	Steady state groundwater flow with varying permeability. Forward and backward particle tracks and conservative and regular particle tracks are generated.
2.4	Transient buoyant flow.	Transient groundwater flow driven by buoyancy via the Boussinesq approximation. Decaying heat source and heat conduction through rock. Transient particle tracks are generated.
2.5	1D Unsaturated flow.	Transient unsaturated groundwater flow. Tested using both Crank Nicholson and Gears Method time stepping.
2.6	Henry's salt transport.	Steady state ground water flow. Density dependent on salinity.
2.7	1D Rock matrix diffusion.	r diffusion between fractured rock and the rock holson and Sequential Iteration solver options.
2.8	1D Nuclide transport with sorption and decay.	Steady state groundwater flow with nuclide transport. Sorption and decay modelled individually and combined. Tested using Crank Nicholson and Fast Linear Transport options.

Table 2-1 CPM verification tests

2.1 Radial Steady State Flow

2.1.1 Overview

This case models steady groundwater flow in a 2D disk where water is removed from the centre at a constant rate and the outer disk boundary is maintained at a constant head.

The example has a simple analytical solution, which is used to verify the ground water flow solution on a range of mesh topologies.

2.1.2 Problem Definition

The problem definition and solution is a variant of that from Feftra [3] and de Marsily [4].

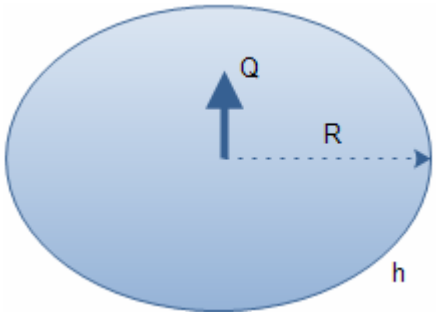

Figure 2-1 Schematic of problem definition

Symbol	Parameter	Value
h	Head at disk circumference	0 m
Q	Outflow from disk	1.0E-7 m^3/s
K	Hydraulic Conductivity	1.0E-8 m/s
R	Radius of disk	2000 m
d	Thickness of disk	1 m
r	Radial distance from axis	0-2000 m

Table 2-2 Input parameters

2.1.3 Variations

2.1.3.1 Mass flux boundary condition

The modelled domain consists of a 15 degree sector, which is truncated at r = 1 m where a mass flux boundary condition is applied. The mesh consists of a line of 3D hexahedral elements, with the spacing refined towards the centre of the domain.

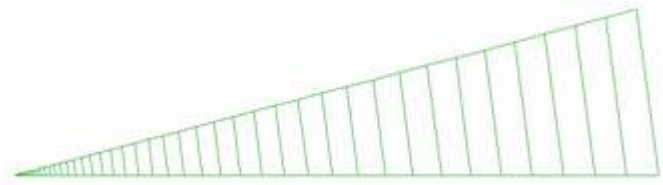

Figure 2-2 Hexahedral mesh with sector truncated close to origin

2.1.3.2 Point sink and prism element

The modelled domain consists of a 15 degree sector, which is composed of a line of hexahedral elements except at the origin where a prism element is used. The outflow is modelled using point sinks at the two vertices on the axis.

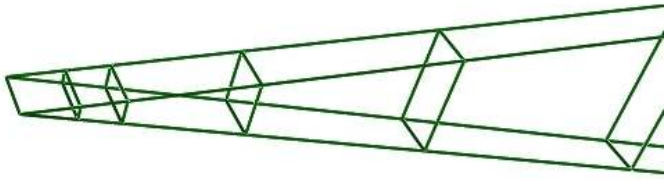

Figure 2-3 Hexahedral mesh with prism at origin

2.1.4 Constrained mesh

The modelled domain consists of a 15 degree sector, which is truncated at r = 1 m, where a mass flux boundary is applied. The mesh consists of a line of 3D hexahedral elements for r = 1 m to r = 1000 m. The mesh is then refined into two cells circumferentially from r = 1000 m to r = 2000 m. The meshes are joined using ConnectFlow constraints. This is an advanced technique that allows grids of different densities to be connected together.

Figure 2-4 Hexahedral constrained mesh

2.1.5 Results

The analytical solution is given by

$$h(r) = h(R) - \frac{Q}{2\pi Kd}\ln(\frac{R}{r})$$

The results from ConnectFlow show very good agreement with the analytical solution in Figure 2-5 and Figure 2-6. The solution for the constrained mesh in Figure 2-7 is a little less accurate as expected.

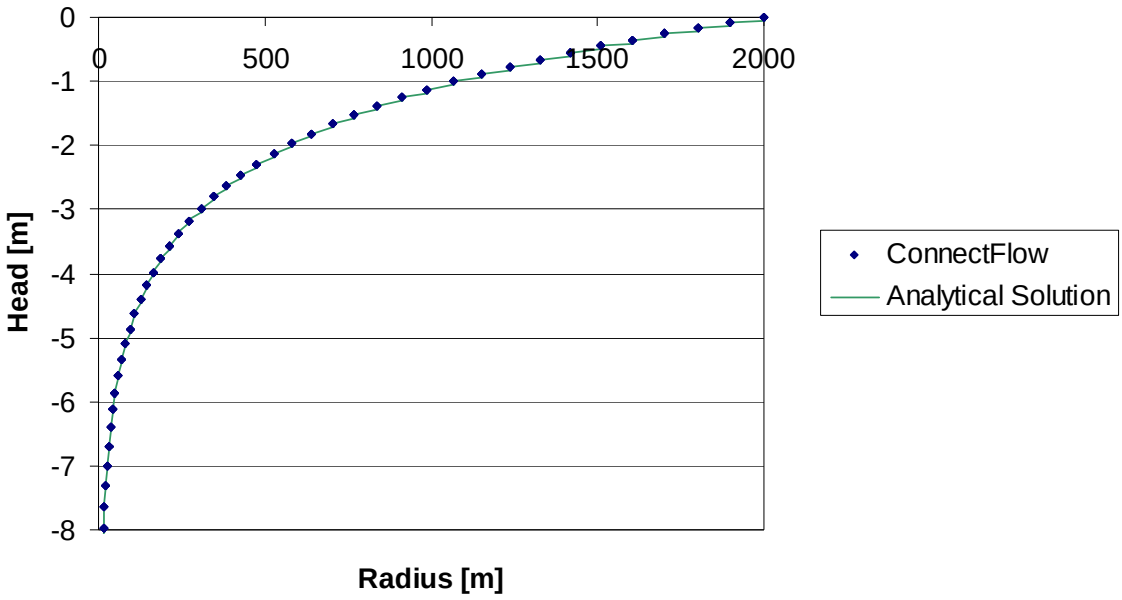

Figure 2-5 Mass flux boundary condition

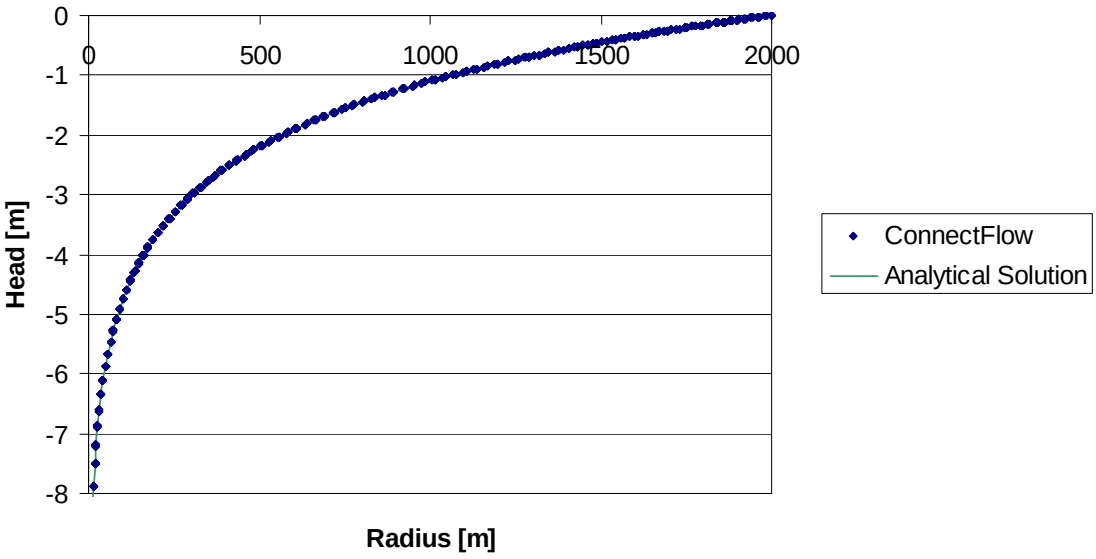

Figure 2-6 Point sink and prism element

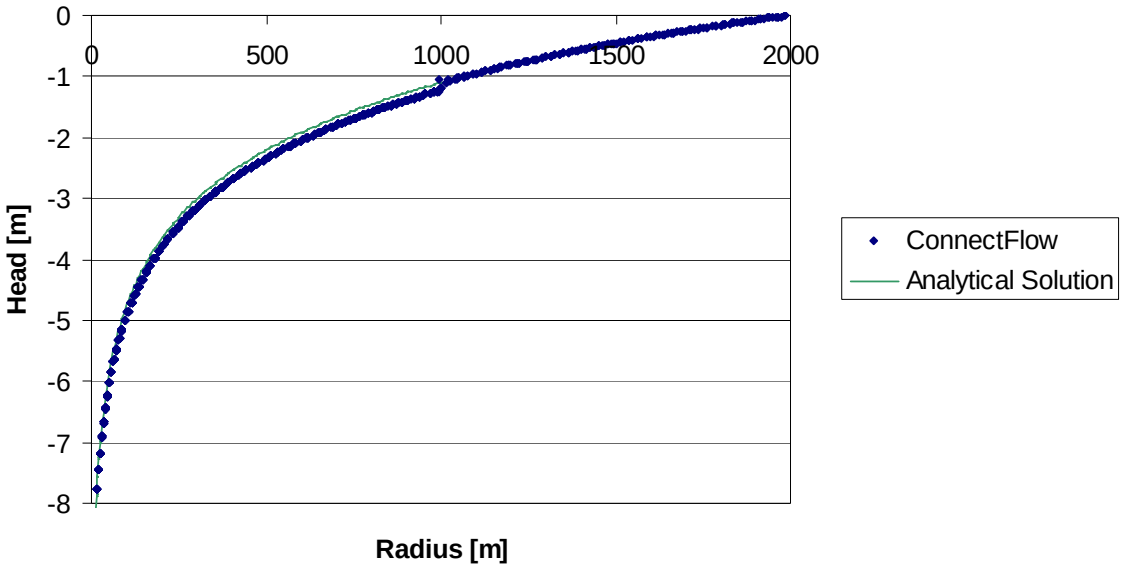

Figure 2-7 Constrained mesh

2.2 Steady Flow in Fractured Rock

2.2.1 Overview

This case is taken from Level 1 of the international HYDROCOIN project for verification of groundwater flow codes [5]. It models steady state flow in a two-dimensional vertical slice of fractured rock. The rock contains two inclined fractures which intersect one another at depth, and have a higher permeability than the surrounding rock.

The topography has been made simple so that it consists of two valleys located where the fracture zones meet the surface. To simplify the problem definition, the shape of the surface is described by straight lines. Although the surface topography is symmetric, the flow is influenced by the asymmetry of the fracture zones.

This problem is based on an idealized version of the hydrogeological conditions encountered at a potential site for a deep repository in Swedish bedrock. A detailed three-dimensional model of this was made in a separate study [6].

2.2.2 Problem Definition

Figure 2-8 depicts the modelled domain.

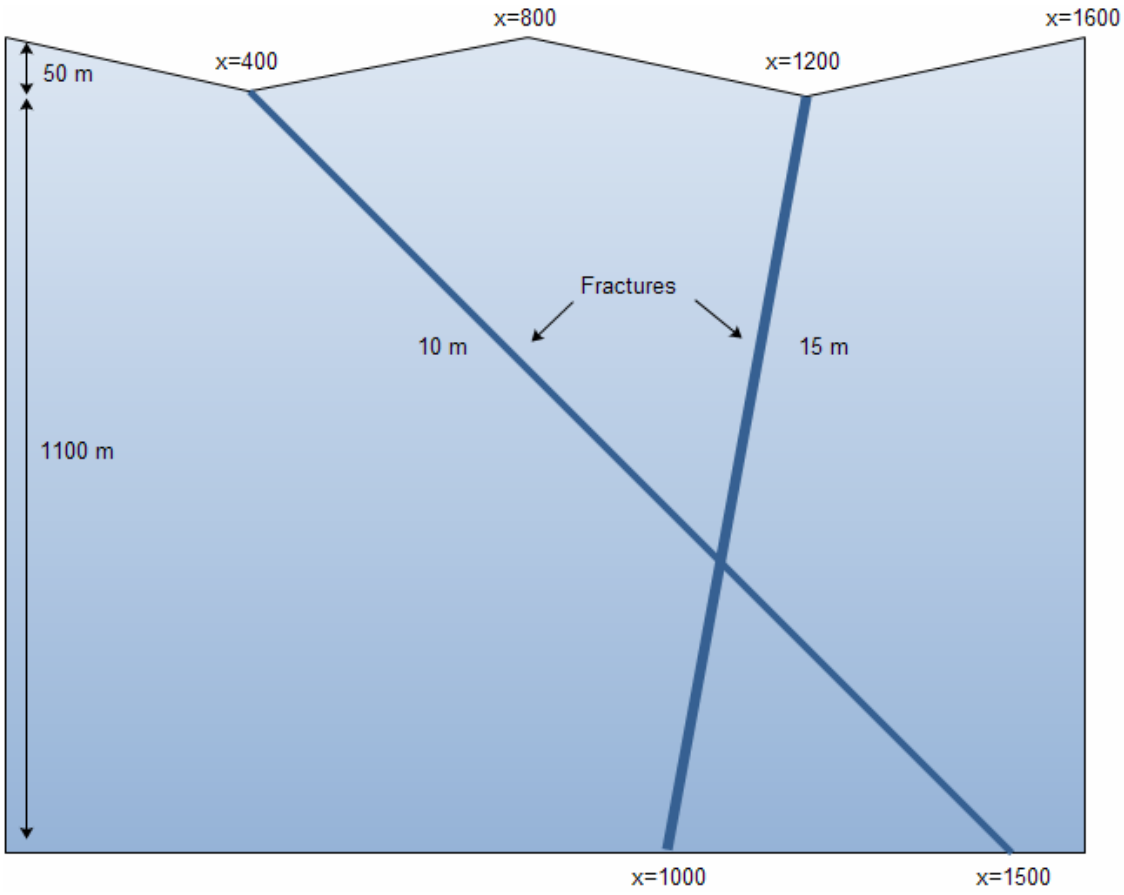

Figure 2-8 Fractured rock

Symbol	Parameter	Value
K_r	Hydraulic conductivity of rock	1.0E-8 m/s
K_f	Hydraulic conductivity of fracture	1.0E-6 m/s
ϕ	Porosity	0.03

Table 2-3 Input parameters

2.2.3 Variations

2.2.3.1 Multiple Element Types

In this variation the region is meshed using a mix of hexahedral (CB27) and prismatic elements as shown in Figure 2-9.

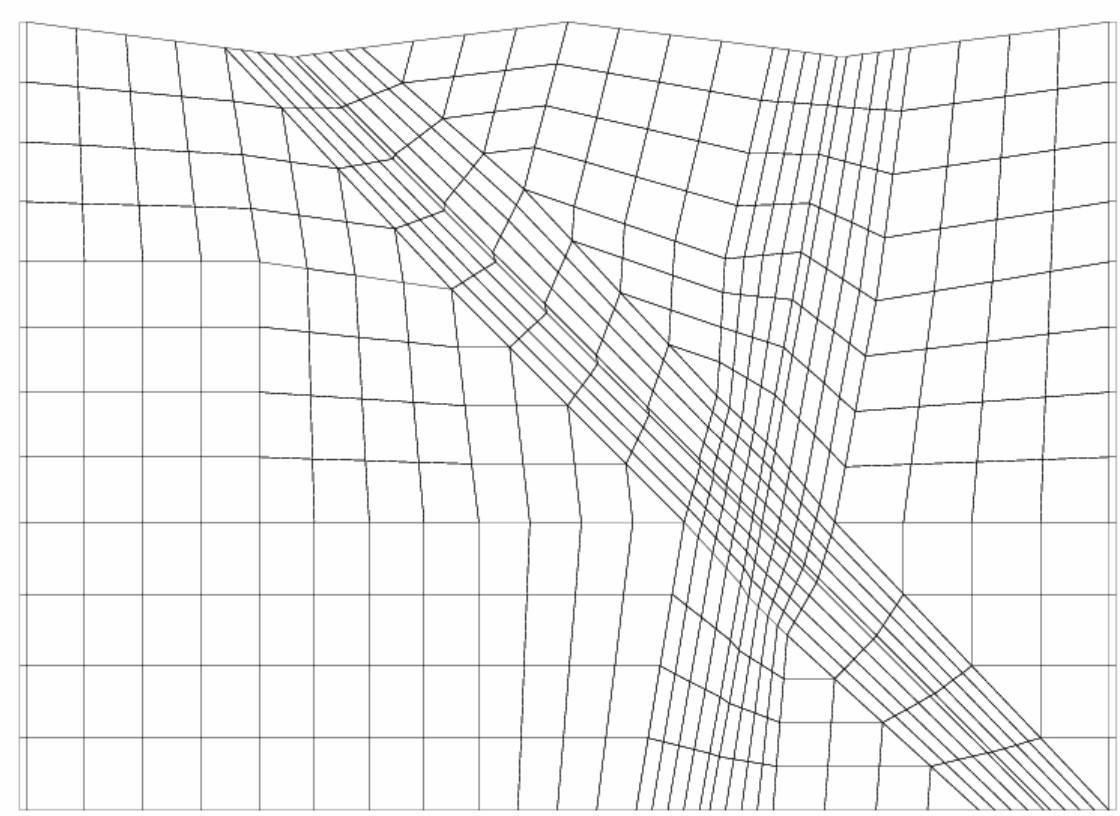

Figure 2-9 Mesh around fractures

2.2.3.2 Hexahedral Elements

In this variant hexahedral elements only are used, and then the element permeabilties are modified according to the imported fractures. It was found that in this scenario the lower order CB08 elements gave a more accurate solution than the CB27 elements for a given mesh resolution. This is likely to be due to the rapid change in permeabilties that are not aligned with the grid.

The results presented here are for mesh with 160x80 elements. The representation of the fractures using this approach is illustrated in Figure 2-10.

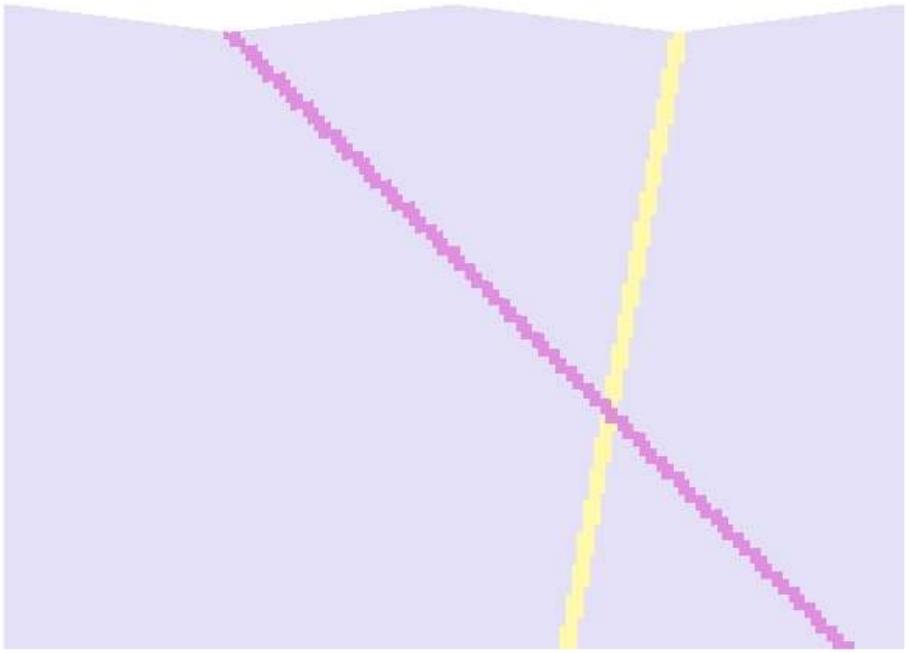

Figure 2-10 Hexahedral elements

2.2.4 Results

The results presented here compare head profile at a height of y=-200. The multiple element type results show excellent agreement with the HYDROCOIN study. The hexahedral element results have a head profile that is close to the HYDROCOIN results, but with slightly higher heads across the range.

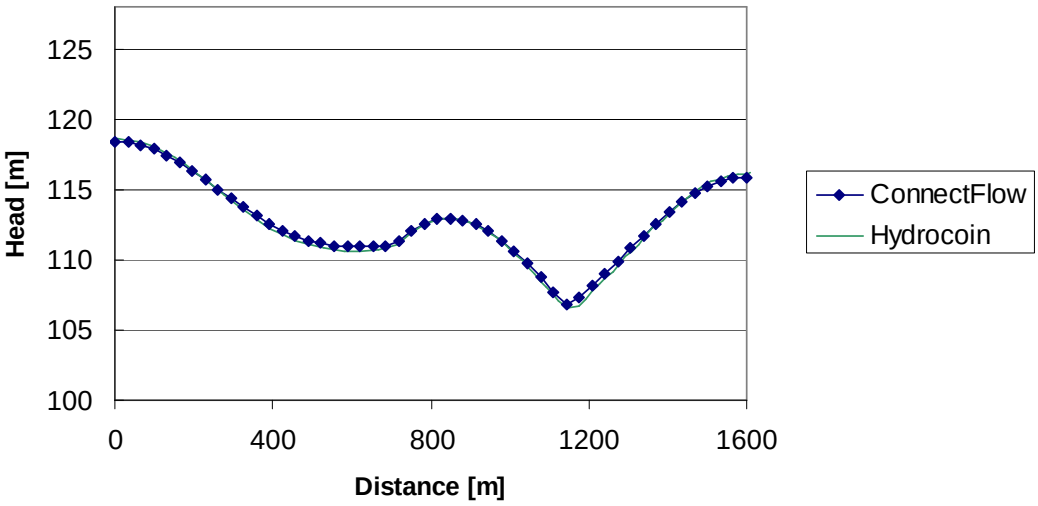

Figure 2-11 Head at height -200m (multiple element types)

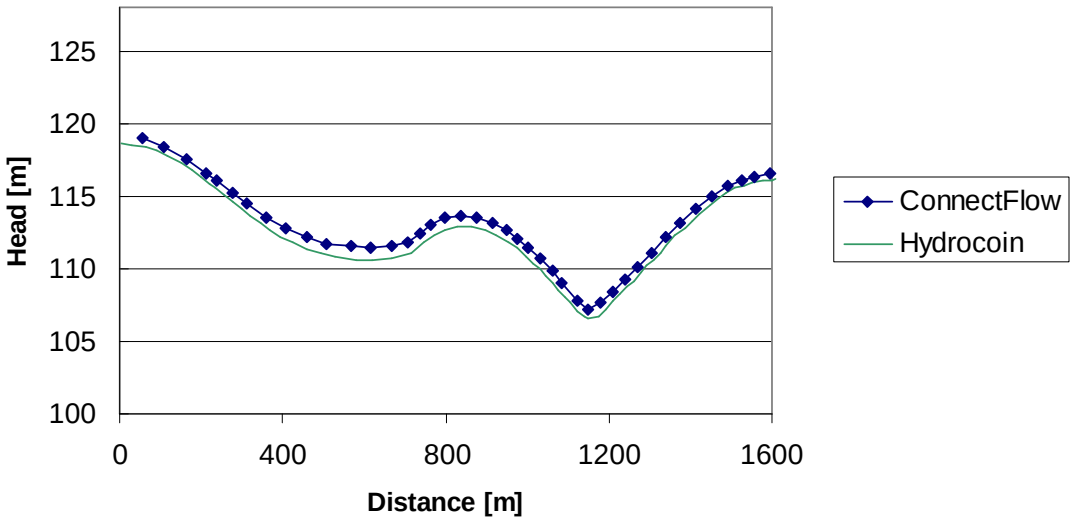

Figure 2-12 Head at height -200m (hexahedral element mesh)

In addition, the ConnectFlow results were compared against the Feftra base case results reported in [3]. The differences in head between the two codes being less than 1% for the multiple element type mesh and less than 2% for the hexahedral mesh (relative to the head variation in the surface boundary condition).

A particle track starting from position (100,-200) also showed good agreement with the Feftra base case, as illustrated in Figure 2-13.

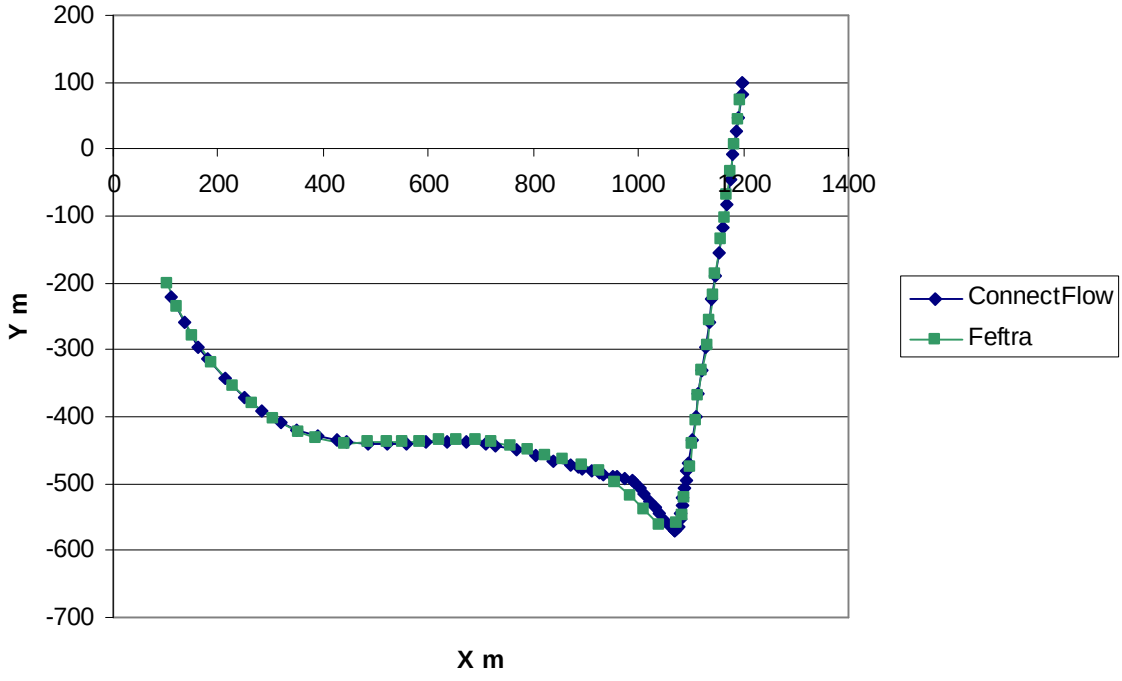

Figure 2-13 Particle track from (100,-200) with multiple element types

In Figure 2-14 the ConnectFlow particle track is overlaid on the geometry, with the track colouring representing elapsed time. The total time of the track is 5% higher than the Feftra base case.

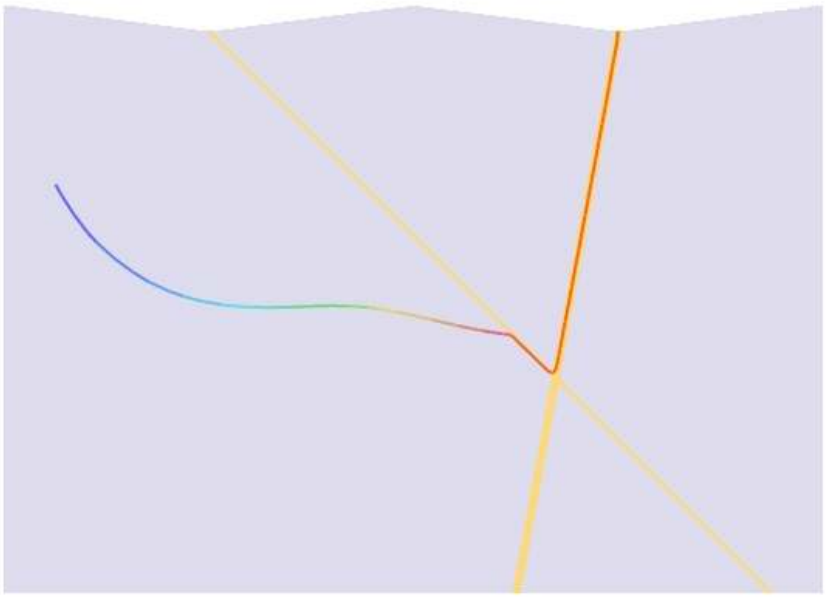

Figure 2-14 Particle track overlaid on geometry

2.3 2D Steady Flow with Particle Tracks

2.3.1 Overview

This case is taken from Level 3 of the international HYDROCOIN project for verification of groundwater flow codes [7]. It models steady state flow in a two-dimensional vertical slice of rock, containing a circular region of higher permeability.

The case has a non-uniform analytical solution and is used in the HYDROCOIN study to test particle tracking.

2.3.2 Problem Definition

The analytical solution assumes an infinite domain for the low permeability region. The original HYDROCOIN setup had a disk radius a = 10m, an outer region Lx = 50m, Ly = 30m and used both calculated and analytically prescribed flow fields.

In the ConnectFlow results presented here both the flow field and particle tracks are calculated. From initial tests it was found that a larger outer region was required in order to appropriately model the analytical solution.

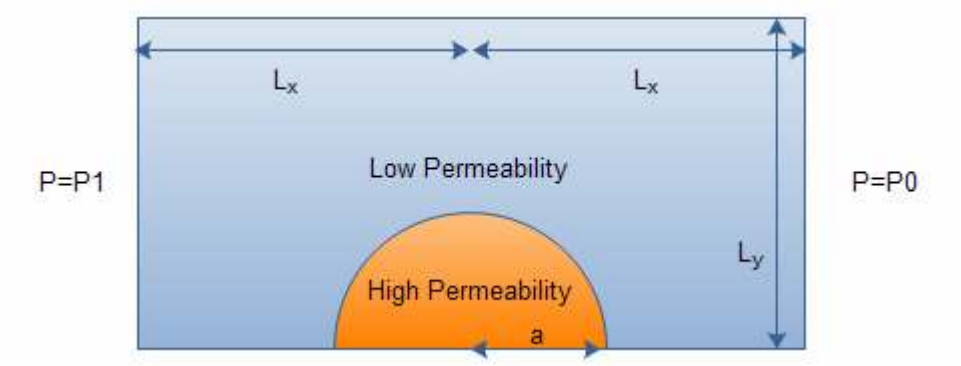

Figure 2-15 Schematic of problem definition

Symbol	Parameter	Value
Lx	Upstream and downstream distances	250 m
Ly	Vertical outer region distance	240 m
a	Radius of inner disk	10 m
P1	Upstream pressure	2.5E5 Pa
P0	Downstream pressure	-2.5E5 Pa
k_o	Permeability of outer region	1.0E-15 m^2
k_i	Permeability of inner region	1.0E-13 m^2
ϕ	Porosity	0.1
ρ	Density	1000 kg/m^3
μ	Viscosity	1.0E-3 Pa.s

Table 2-4 Input parameters

Eight particle tracks are released 50 m upstream of the disk centre and at Y values of 10, 12, 14, 16, 18, 20, 22 and 24 m.

The analytical solution for the pathlines is given in the HYDROCOIN report [7] as

$$y = y_o / (1 + \frac{a^2}{r^2} \frac{(k_i - k_o)}{(k_i + k_o)})$$ for r > a

$$y = y_o \frac{(k_i + k_o)}{2k_o}$$ for r < a

Where r is the distance from the center of the disk and y_0 is a constant representing the height of the track a long distance away from the origin.

2.3.3 Variations

2.3.3.1 Wrapped Mesh

In this variation, the mesh is modelled to wrap around the cylinder. A higher quality mesh is generated, but some vertices are surrounded by 3 elements and others by 5. A mesh of around 3000 elements was used.

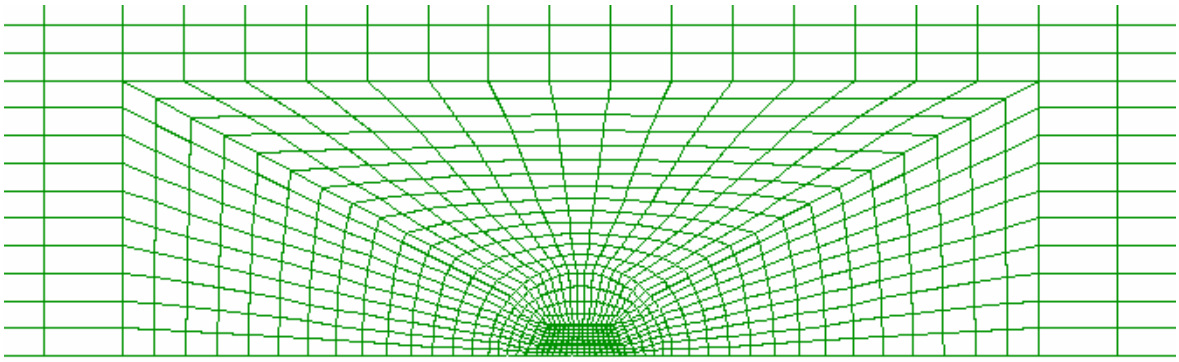

Figure 2-16 Wrapped mesh

2.3.3.2 Regular Mesh (Distorted Elements)

In this variation a regular mesh is used where elements always have 4 neighbours, which results in a distorted mesh inside the cylindrical region. A mesh of around 6000 elements was used. The mesh is finer in this case, as the refinement of the cylinder propagates to the boundaries.

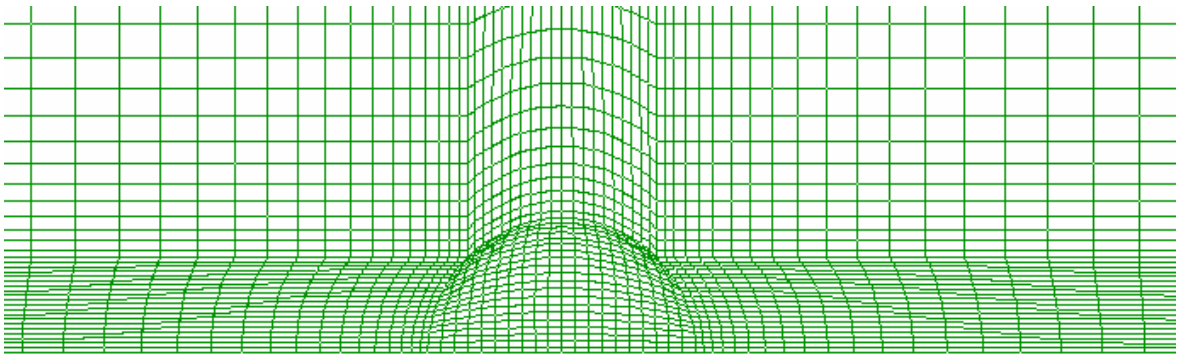

Figure 2-17 Regular mesh

2.3.4 Results

The calculated particle tracks were within 1% of the analytical solution, both in terms of location at each point and in terms of overall travel from x = -50m to x = +50m.

Calculation method	% Error in Location	% Error in Travel Time
Wrapped mesh, regular tracks	0.96%	0.44%
Regular mesh, regular tracks	0.41%	0.17%

Table 2-5 Particle tracking results

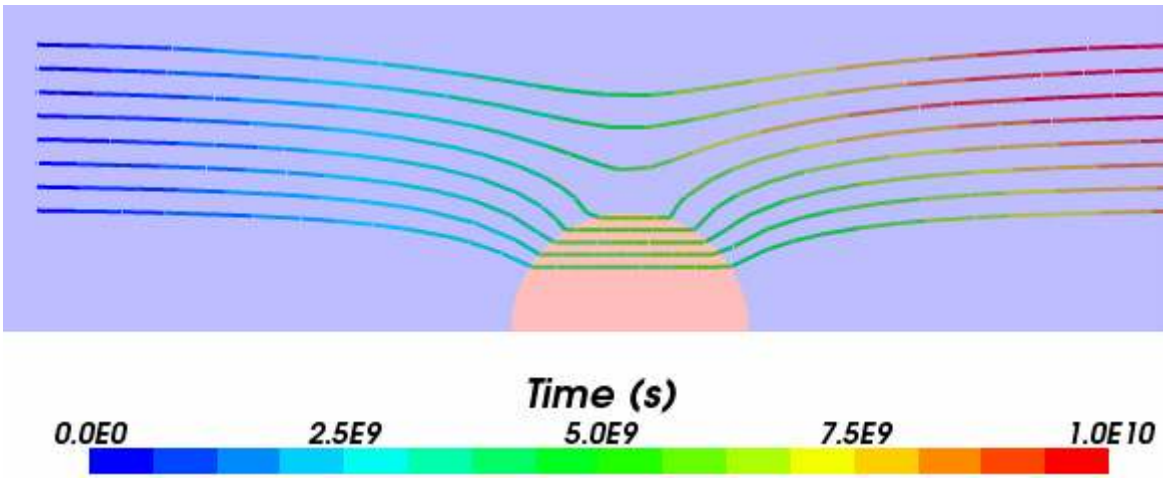

Figure 2-18 Particle tracks for wrapped mesh

In addition, the volumetric flow rate through the inner disk was calculated for variation 1, using the "calculate conserved mass flux" option.

The flow through the disk from [7] has a constant velocity in the X direction of $\frac{k_o k_i}{(k_i + k_o)} \frac{(P1 - P0)}{2L_x \mu\varphi}$.

For the values in Table 2-4, this gives a flow rate of 1.9801E-7 m^3/s. The calculated ConnectFlow value is 1.9834E-7 m^3/s which is within 1% of the analytical solution.

2.4 Transient Buoyant Flow

2.4.1 Overview

This case is taken from Level 1 of the international HYDROCOIN project for the verification of groundwater flows [5]. It models the flows arising from an exponentially decaying heat source and has an analytical flow solution.

This type of problem is relevant when considering the disposal of heat emitting radioactive waste, where buoyancy induced flows can last for thousands of years.

2.4.2 Problem Definition

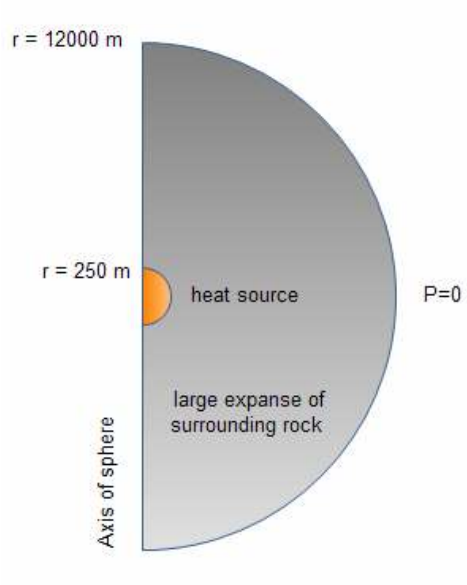

Figure 2-19 Schematic of problem definition

The test problem models transient heat flow through the rock only and ignores advection of heat. The viscosity is taken to be constant and the density variation is only applied to the buoyancy term of the equations.

The modelled domain consists of a thin one cell thick segment of the sphere. The analytical solution assumes an unbounded region of surrounding rock. Following some initial test runs, a surrounding region of 12000 m was selected as having a minimal impact on the solution.

A relatively fine mesh of 26000 elements was used. Coarser meshes of around 5000 elements give good results for the temperature and pressure profiles but have larger errors on particle tracking positions and travel times.

Symbol	Parameter	Value
W_0	Initial power output	250 MW
λ	Decay constant in heat source	7.3215E-10 1/s
ρ_r	Rock density	2.6E3 kg/m^3
C	Rock specific heat	8.79E2 J/kg K
Γ_r	Rock thermal conductivity	2.51 W/m K

k	Permeability	1.0E-16 m^2
ϕ	Porosity	1.0E-4
S_s	Specific storage coefficient	2.0E-6 1/m
ρ	Density	992.2 kg/m^3
μ	Viscosity	6.529E-4 Pa.s
β	Expansion coefficient of water	3.85E-4 1/K

Table 2-6 Input parameters

2.4.3 Results

The comparison of results includes temperature profiles Figure 2-20, pressure profiles Figure 2-21 and transient particle tracks Figure 2-22 and Figure 2-23.

The results are all within 7% of the analytical solution, including the particle travel times.

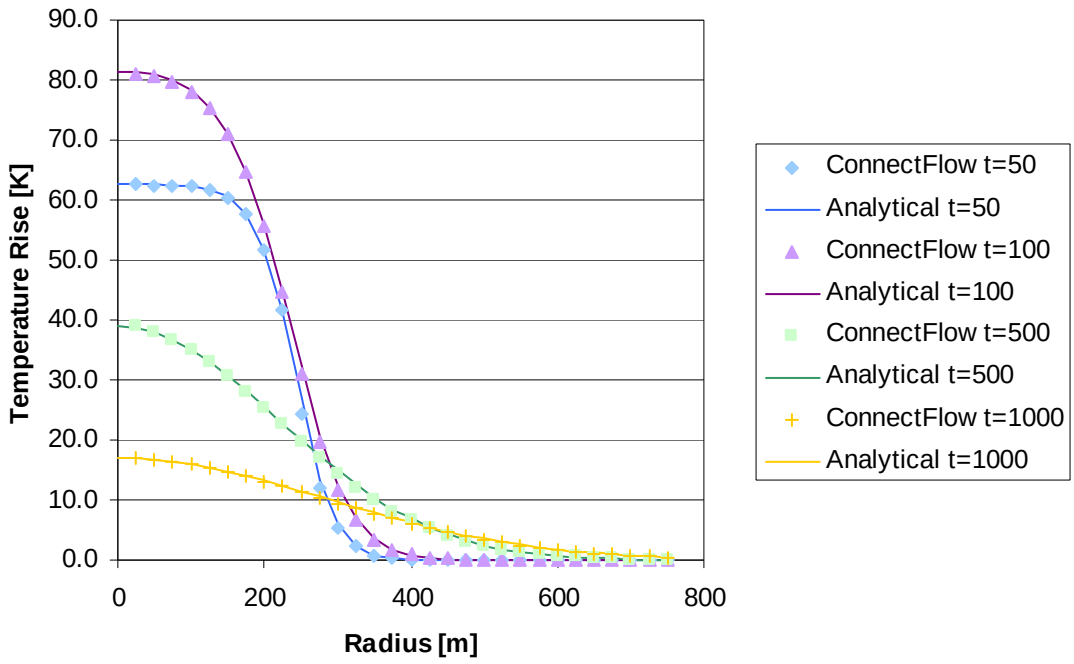

Figure 2-20 Vertical temperature rise along the vertical sphere centreline

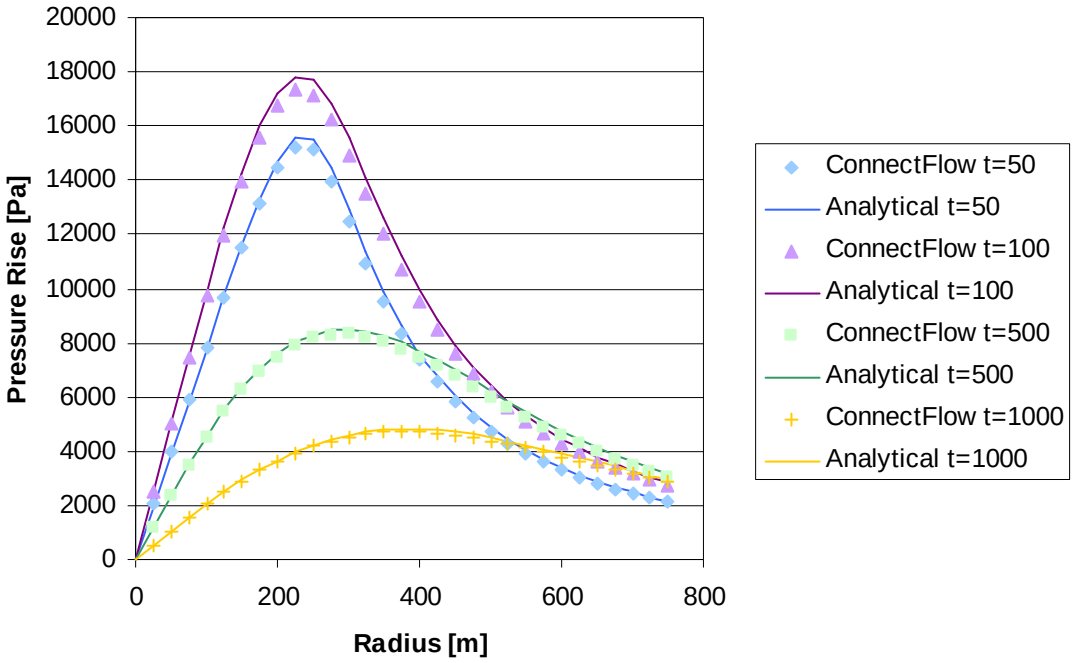

Figure 2-21 Vertical pressure rise along the vertical sphere centreline

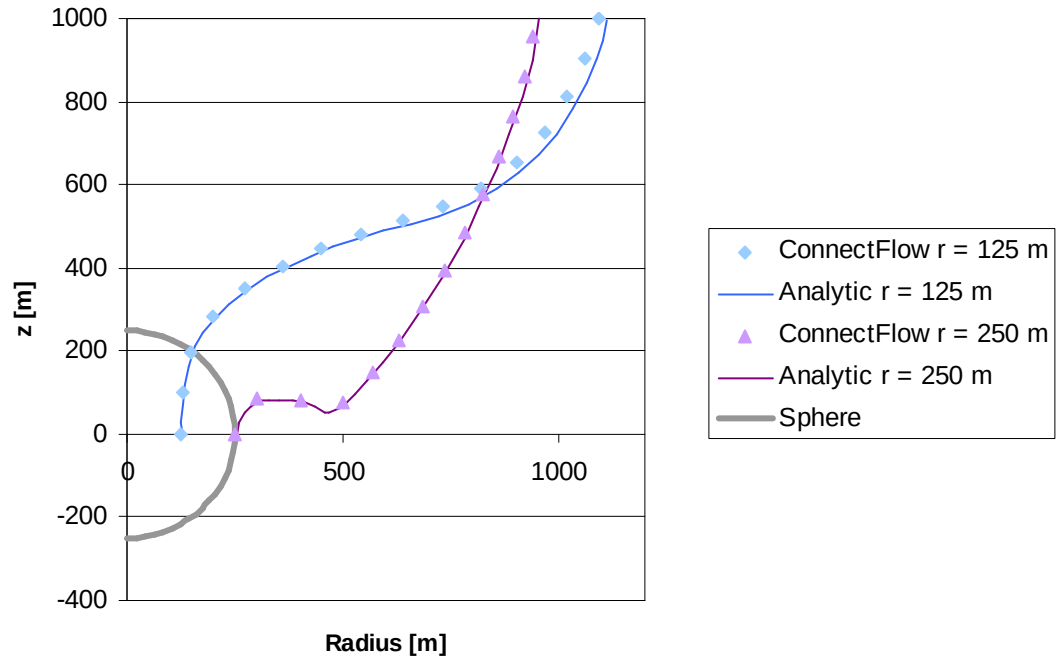

Figure 2-22 Particle tracks originating from z = 0 starting at t = 100 years

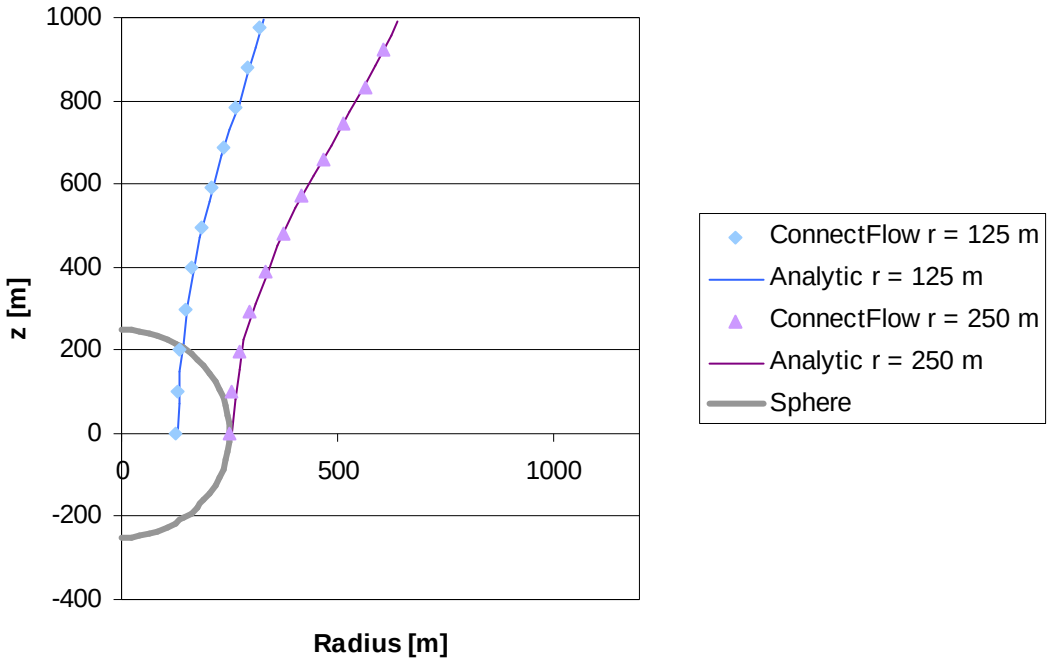

Figure 2-23 Particle tracks originating from z = 0 starting at t = 1000 years

2.5 1D Transient Unsaturated Flow

2.5.1 Overview

This case models transient flow in a 50 m horizontal section of clay, where the initial pressure is constant and the ends are maintained at a different pressure.

For small variations in pressure the problem has a semi-analytical solution.

2.5.2 Problem Definition

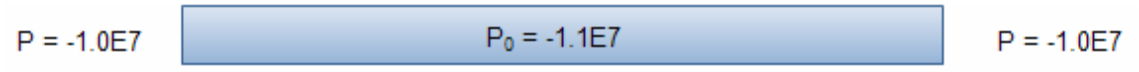

Figure 2-24 Schematic of problem definition

The region was meshed using a line of 40 hexahedral elements.

The unsaturated behaviour for relative permeability and capillary pressure were modelled using Van Genuchten functions.

Symbol		Parameter	Value
K		Hydraulic Conductivity	5.0E-14 m/s
ϕ		Porosity	0.18
S_s		Specific storage coefficient	2.0E-6 1/m
ρ		Density	1000 kg/m^3
μ		Viscosity	1.0E-3 Pa.s
Van Genuchten	n	Exponent	1.5
	Pr	Entry pressure	8.0E6 Pa
	S_{lr}	Residual Saturation	0.01

Table 2-7 Input parameter values

As the variation in saturation across the model is small (<3%), we can approximate the equations for transient unsaturated flow as a diffusion equation, so that, in 1D

$$\frac{\partial P}{\partial t} = \alpha \frac{\partial^2 P}{\partial x^2}$$

where

α is the diffusivity [m^{2}s^{-1}];
x is distance [m];
P is pressure;
t is time.

and α is given by

$$\alpha = \frac{k_r K}{S_s S + \phi \rho g \frac{\partial S}{\partial P}}$$

where S is the liquid saturation and k_r is the relative permeability and g is gravity.

For the case considered here, the values in the above equation are averaged between the initial conditions and the boundary conditions to provide an approximate constant diffusivity.

Given this approximate constant diffusivity, a semi-analytical solution can be obtained from

$$P = P_1 + (P_0 - P_1)\sum_{n=0}^{\infty} \frac{4}{(2n+1)\pi} \exp\left\{\frac{-(2n+1)^2 \pi^2 \alpha t}{L^2}\right\} \sin\left\{\frac{(2n+1)\pi x}{L}\right\}$$

Where P_0 is the uniform initial pressure field -1.1E7, P_1 the boundary pressure of -1.0E7, and L the domain length of 50 m.

2.5.3 Variations

2.5.3.1 Crank Nicholson

The transient behaviour is modelled using Crank Nicholson with 150 time steps of size 1.0E11 seconds.

2.5.3.2 Gears method

The transient behaviour is modelled using Gears predictor-corrector time stepping method with an initial time step of 1.0E11 seconds. A total of 23 time steps were used.

2.5.4 Results

The results show good agreement with the semi-analytical solution. The small differences are due to the semi-analytical model assuming constant saturation with time.

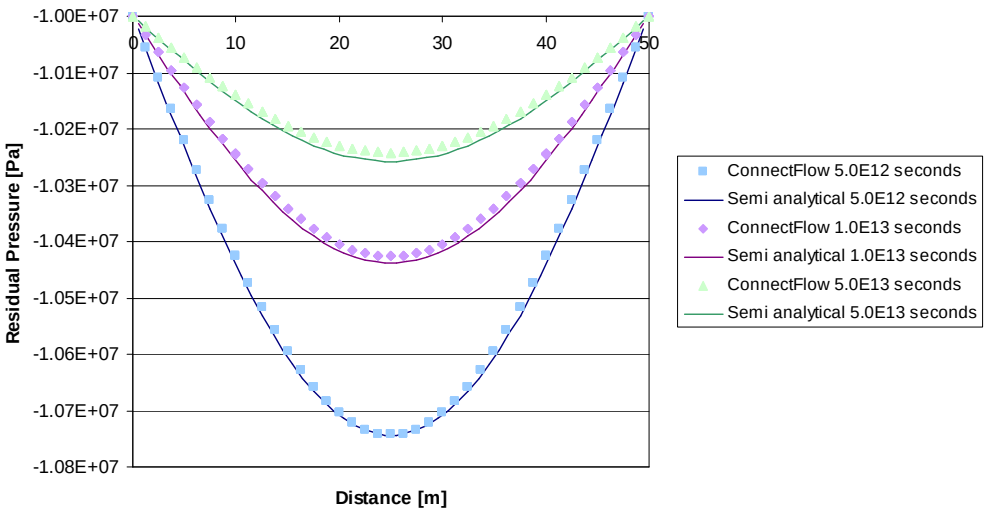

Figure 2-25 Crank Nicholson - Transient unsaturated pressures

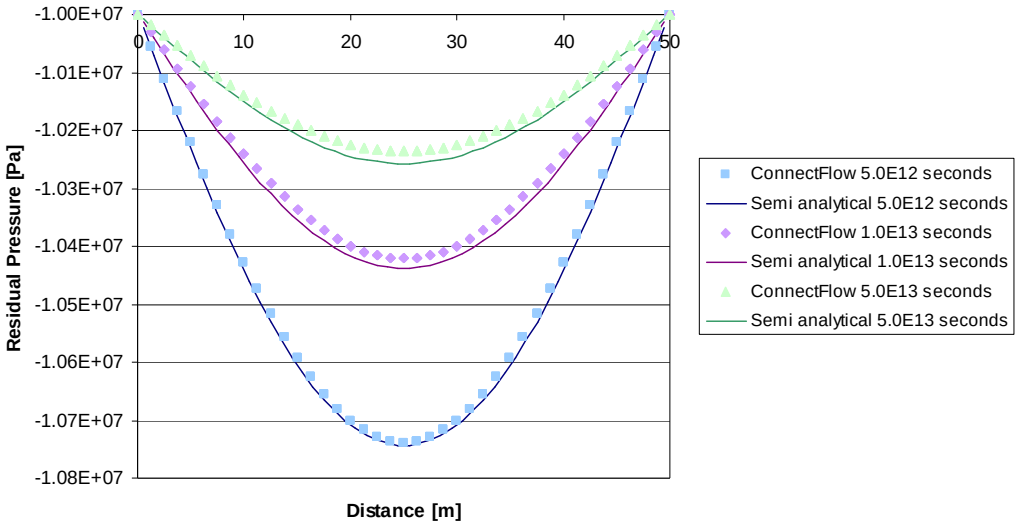

Figure 2-26 Gears method - Transient unsaturated pressures

An additional comparison was made with Tough2v2 software [8].

Calculation method	Pressure at x=25, t=1.0E13
ConnectFlow – Crank Nicholson	-1.0426E7
ConnectFlow – Gears Method	-1.0421E7
Semi analytical	-1.0438E7
Tough2	-1.0423E7

Table 2-8 Comparison with Tough2v2

Both ConnectFlow and Tough2 show the same behaviour relative to the semi analytical solution.

2.6 Henry's Salt Transport

2.6.1 Overview

This case considers salt water intrusion into a vertical slice of an isotropic homogeneous confined aquifer.

The variant modelled is a modified version of the original Henry's test case, as recommended in [9]. The modified case halves the fresh water inflow rate, which increases the sensitivity of the solution to the variation in density.

2.6.2 Problem Definition

A schematic of the test case is shown in Figure 2-27 and the input parameters are given in Table 2-9.

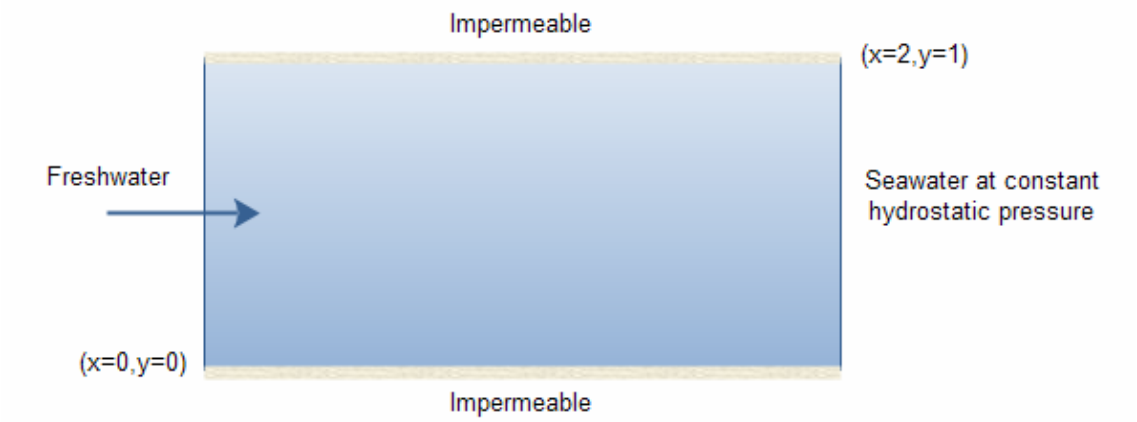

Figure 2-27 Henry's Problem

A uniform hexahedral grid was used of size 80x40 elements.

Symbol	Parameter	Value
K	Hydraulic conductivity of rock	1.0E-2 m/s
D	Coefficient of molecular diffusion	1.886E-5 m^2/s
Q	Freshwater inflow per unit depth	3.3E-5 m^2/s
ρ_0	Reference density	998 kg/m^3
ρ_{max}	Saltwater density	1023 kg/m^3
α_L	Longitudinal dispersivity	0 m
α_T	Transverse dispersivity	0 m
ϕ	Porosity	0.35

Table 2-9 Input parameters

The model makes use of the ConnectFlow "reference waters" capability which allows fluids with different properties to be defined. The steady solution is obtained by running a transient solution until the steady state is reached.

2.6.3 Results

The test case has an analytical solution, represented by an infinite double Fourier series. A truncated form of the series gives a non-linear system which can then be iteratively solved. Results from this process are reported in [9] and these are used for the comparisons in Figure 2-28. The maximum error in contour location is less than 3%.

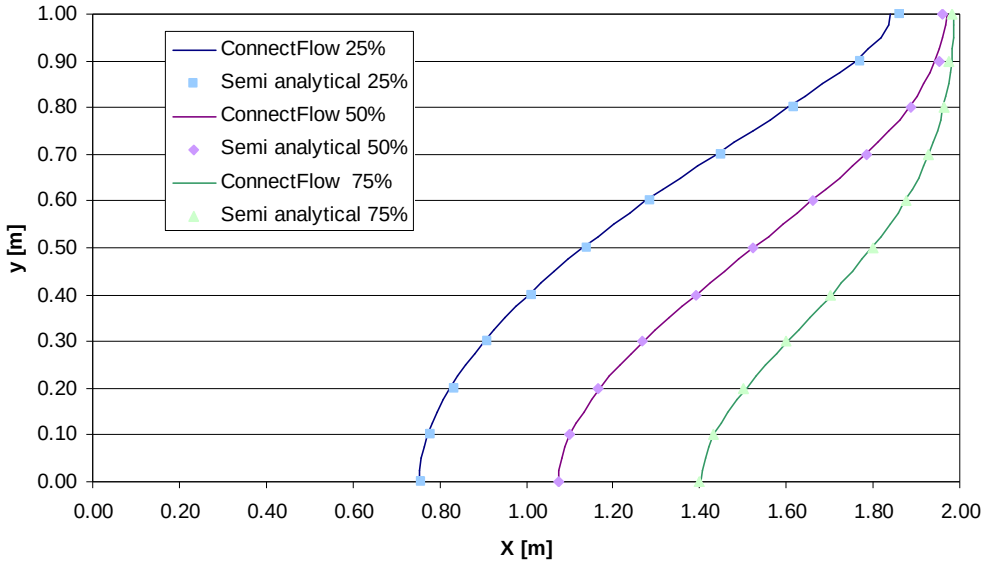

Figure 2-28 Non-dimensional concentration of salinity

2.7 1D Rock Matrix Diffusion (RMD)

2.7.1 Overview

This case considers the transient one dimensional transport of salinity through fractured rock where diffusion between the fractured rock and the adjacent rock matrix is modelled. This test case assumes a constant density.

The test case is taken from the SKB R-04-78 report [10] and has a semi-analytical solution.

2.7.2 Problem Definition

Figure 2-29 depicts the modelled 1D domain.

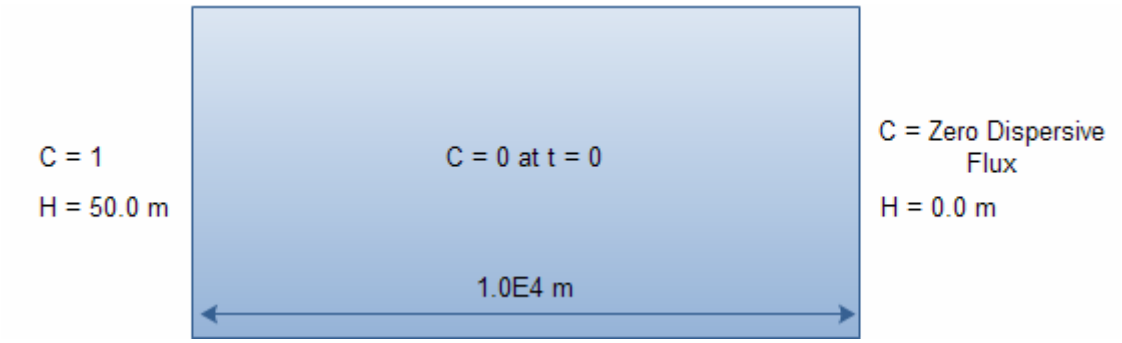

Figure 2-29 Schematic of problem definition

Symbol	Parameter	Value
k	Rock permeability	1.0E-11 m^2
D	Salt diffusion coefficient	1.0E-9 m^2/s
ρ	Density	998.3 kg/m^3
ρ_{max}	Saltwater density	998.3 kg/m^3
α_L	Longitudinal dispersivity	100 m
α_T	Transverse dispersivity	10 m
ϕ	Fracture porosity	0.01
μ	Viscosity	1.0E-3 Pa.s
τ	Tortuousity	1.0
ϕ_m	Matrix porosity	0.1
D_i	Intrinsic diffusion coefficient	5.0E-11 m^2/s
σ	Fracture surface area per unit volume.	2 m^{-1}

Table 2-10 Input parameters

In this case the rock matrix diffusion slows down the increase in salinity in the fractured rock, as a proportion of the salinity is diffusing into the surrounding rock matrix. The time taken for the mid-point relative concentration to reach 0.99 is increased by more than a factor 10 due to RMD.

2.7.3 Variations

2.7.3.1 Crank Nicholson

In this variation the non-linear system is solved using Newton iteration on each time step for all variables as a single group. Automatic time stepping is used to gradually increase the time step size from its initial value of 1.0E6 seconds.

2.7.3.2 Sequential Inner Iteration

Sequential inner iteration solves the non-linear system of equations that arise at each time step according to a user-specified sequence of Newton iterations on subgroups of the full system of equations. In this test the pressure field is time independent, so just the salt concentration is solved for.

This setup also uses nodal quadrature in order to allow an optimized fast equation assembly process. Both the fast assembly and normal assembly were tested.

Automatic time stepping is used to gradually increase the time step size from its initial value of 1.0E6 seconds.

2.7.4 Results

The semi-analytical solution is derived using Laplace transforms, which are then inverted numerically. The details of this process are covered in [10].

The results show good agreement with the semi-analytical solution, the ConnectFlow concentrations being within 1% of the semi-analytical solution for all variations. The concentration profiles for three time values are shown in Figure 2-30.

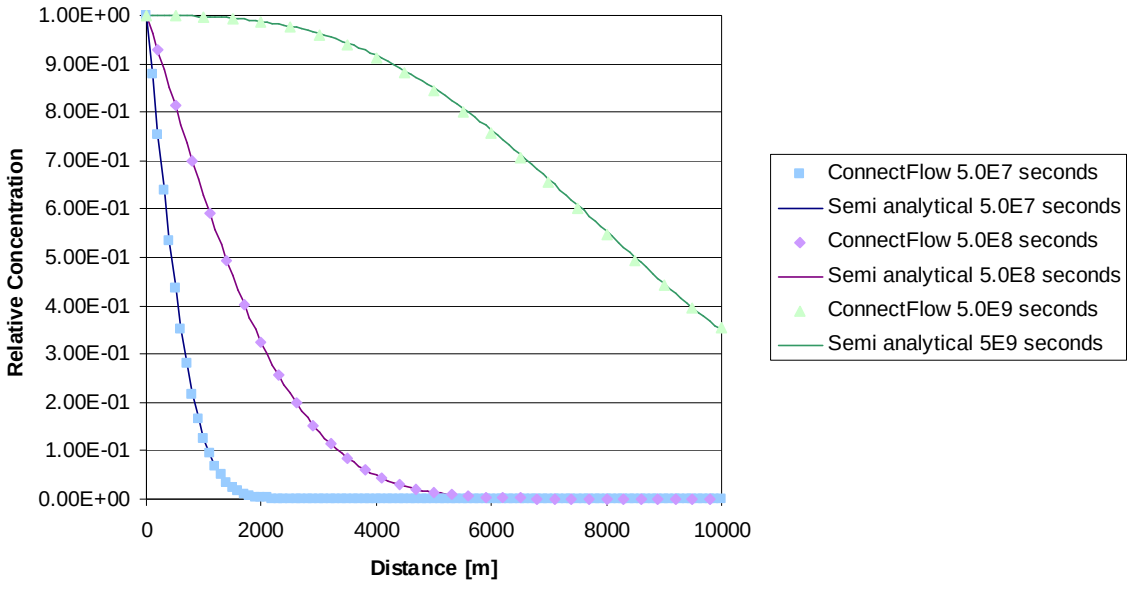

Figure 2-30 Crank Nicholson - Relative concentration

2.8 1D Nuclide Transport with Sorption and Decay

2.8.1 Overview

This case considers transient one-dimensional nuclide transport due to advection and diffusion. Both sorption and decay are considered.

The test case is taken from [11] and has an analytical solution.

2.8.2 Problem Definition

Figure 2-29 depicts the modelled 1D domain.

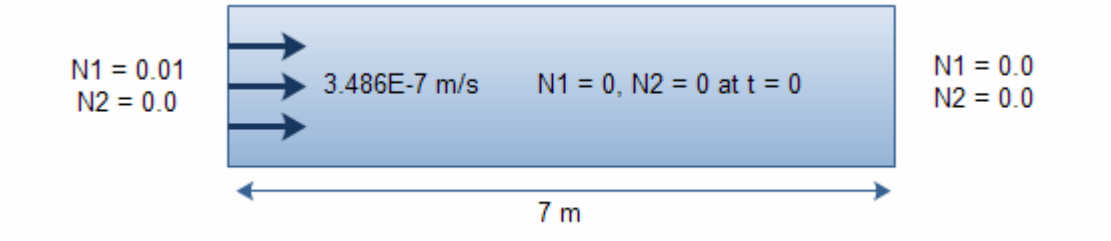

Figure 2-31 Schematic illustration of the problem definition

Symbol	Parameter	Value
k	Rock permeability	1.24E-9 m^2
U	Darcy velocity	3.486E-7 m/s
D	Nuclide diffusion coefficient	1.162E-7m^2/s
α_L	Longitudinal dispersivity	0 m
α_T	Transverse dispersivity	0 m
R_{n1}	Retardation factor nuclide 1	2.0
R_{n2}	Retardation factor nuclide 2	1.0
λ_{n1}	Decay constant nuclide 1	4.011E-7 1/s
λ_{n2}	Decay constant nuclide 2	1.0E-20 1/s
τ	Tortuousity	1.0
ρ	Density	1000.0 kg/m^3
μ	Viscosity	1.0E-3 Pa.s
ϕ	Porosity	0.3

Table 2-11 Input parameters

Constant pressure boundary conditions are applied to generate the desired Darcy velocity. The timescale modelled is 20 days which also corresponds to the half life of the parent nuclide N1.

The mesh consists of 100 CB08 elements along the length of the flow domain, and the time step is taken to be 1E4 seconds.

2.8.3 Variations

2.8.3.1 Fast Linear Transport

Four runs are carried out to illustrate the effect of sorption and decay on the solution.

- No decay or sorption
- Sorption only
- Decay only
- Sorption and decay

2.8.3.2 Crank Nicholson

This variation repeats the sorption and decay case using the Crank Nicholson transient solver.

2.8.4 Results

The results show excellent agreement with the analytical solution [12]. The concentration of the parent nuclide N1 is compared with the analytical solution for each of the four fast linear transport runs in Figure 2-32, Figure 2-33, Figure 2-34 and Figure 2-35.

The Crank Nicholson results were very close to the Fast Transient results, with the peak daughter nuclide concentration being 1% higher and the parent nuclide concentration being identical.

Figure 2-36 shows the ConnectFlow daughter nuclide N2 concentration for the sorption and decay case.

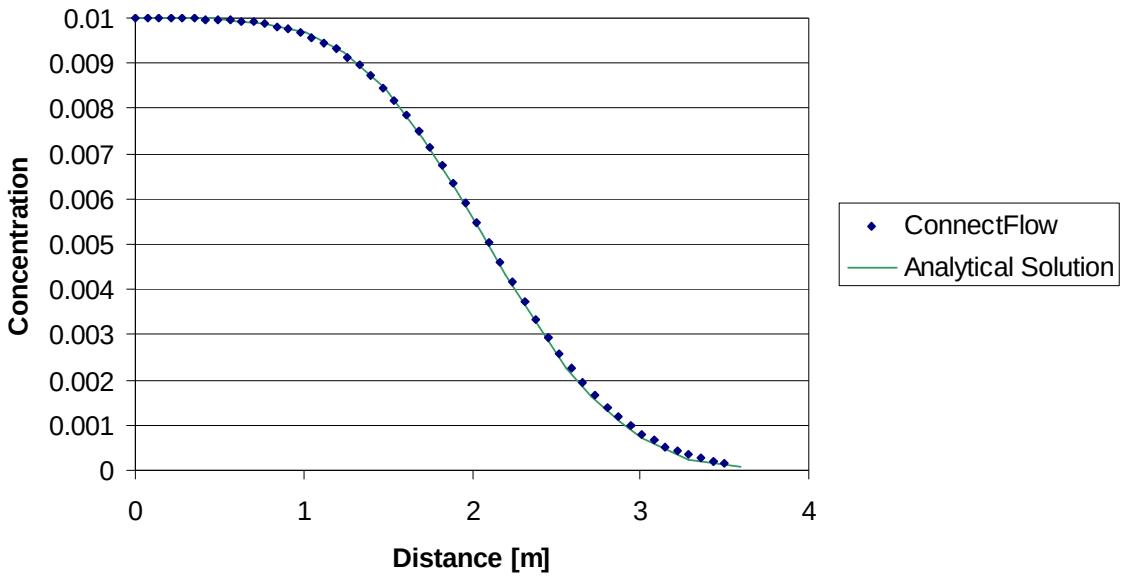

Figure 2-32 N1 concentration with no sorption or decay

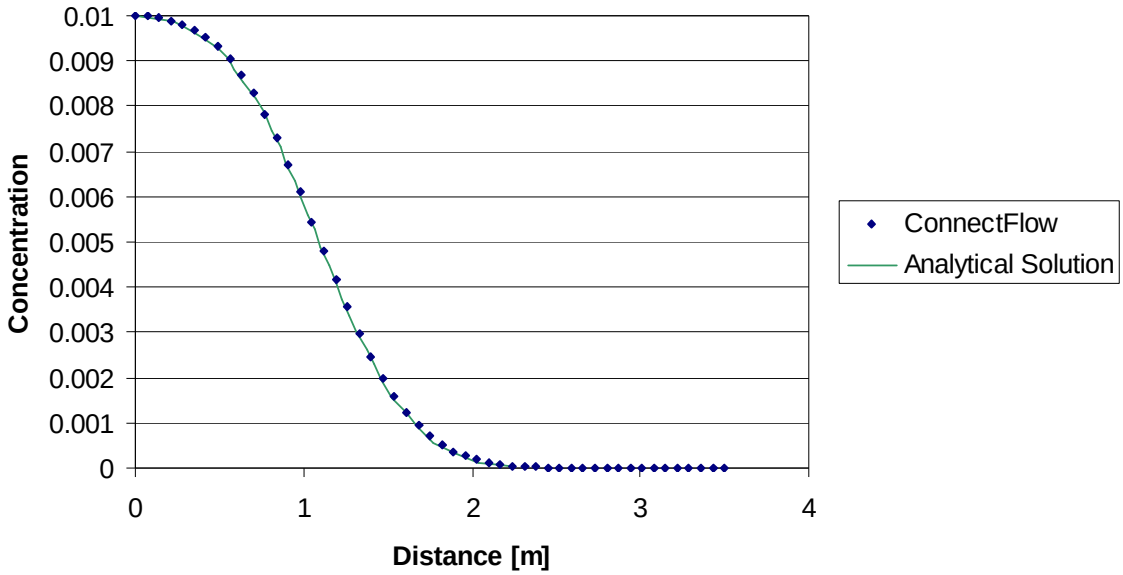

Figure 2-33 N1 concentration with sorption only

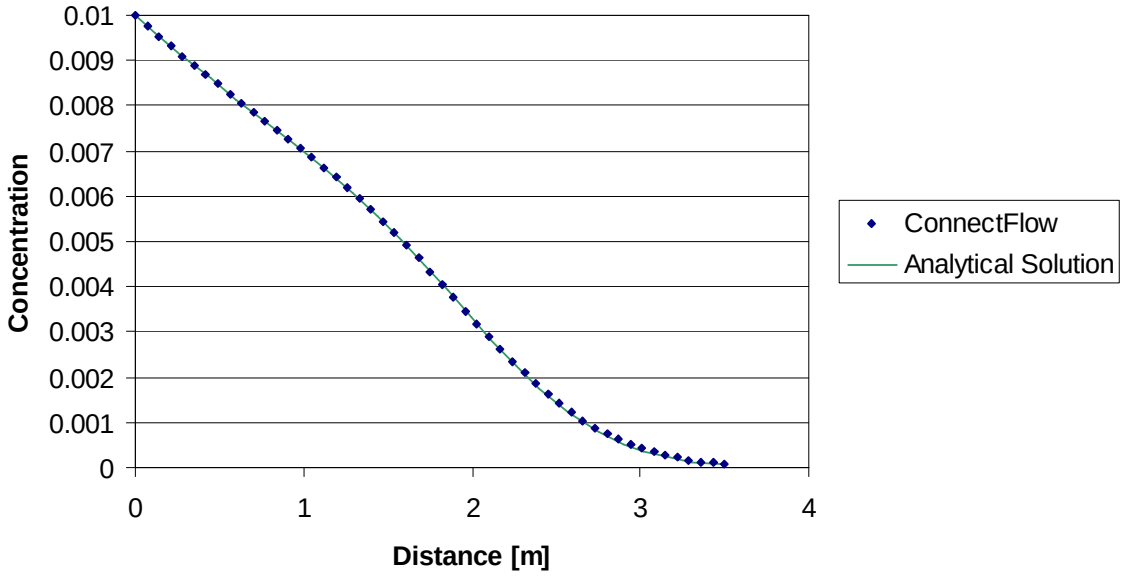

Figure 2-34 N1 concentration with decay only

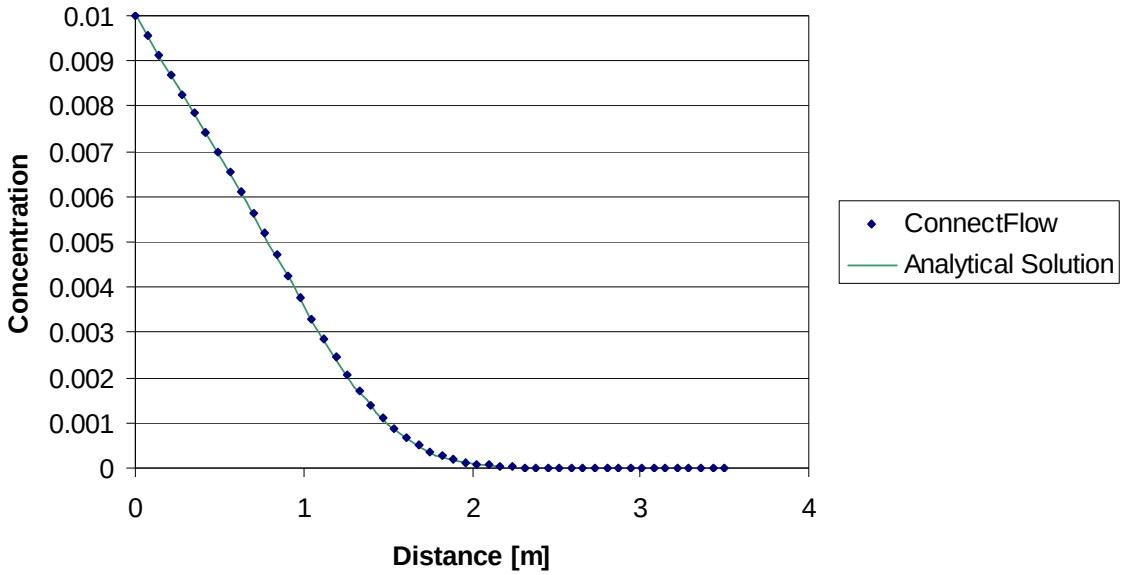

Figure 2-35 N1 concentration with both sorption and decay

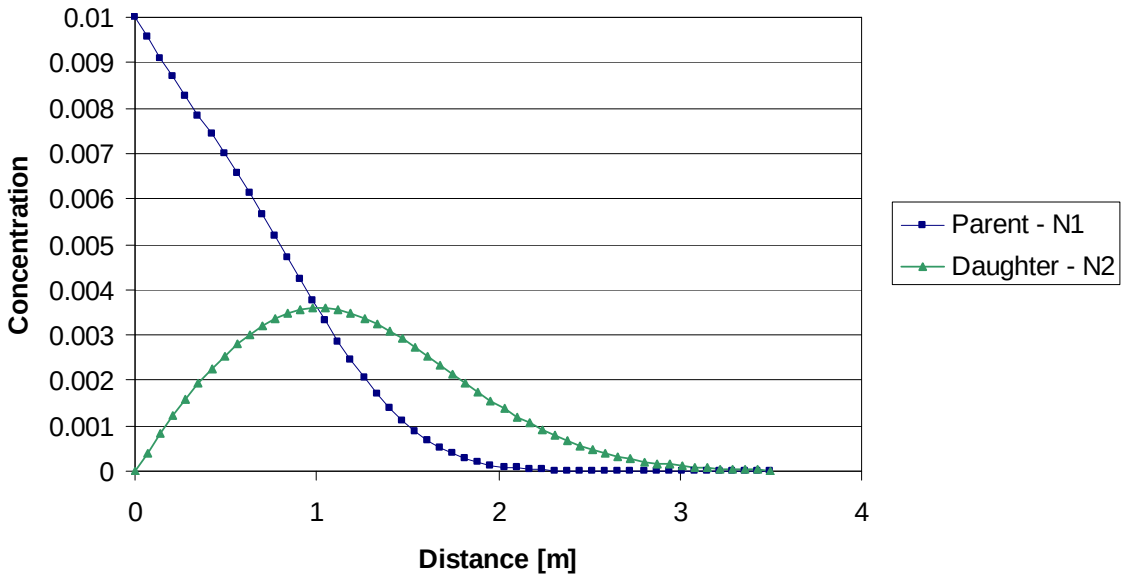

Figure 2-36 Parent and daughter concentrations for the sorption and decay case

3 Discrete Fracture Network Verification

A summary of the DFN test cases is given in Table 3-1.

Case	Title	Overview
3.1	3D Fracture distributions	Generation and export of random fractures. The exported fractures are analysed to check the orientation and side length against the expected values.
3.2	3D Fracture connectivity.	Evaluation of the critical areal density in connecting 1 m square fractures, with a uniform distribution of orientations within a cube.
3.3	3D Fracture connectivity, power law distribution.	Evaluation of the critical areal density as a function of domain size for square fractures with a power law distribution exponent of 2.5 for fracture size and uniform distribution for orientation.
3.4	Upscaling from DFN to CPM.	Calculation of permeability distribution from a DFN model with and without guard zones. Import of permeability data into CPM model. Comparison of steady state flow distributions.
3.5	Radial steady state flow.	Steady state groundwater flow with a borehole used to apply the required mass flow boundary condition.
3.5	Three fracture intersections.	Steady state groundwater flow between three intersecting fractures. Forward and backward particle tracks are generated.
3.7	Steady state flow in fractured rock.	Steady state groundwater flow through intersecting fractures within a rock matrix. Rock matrix is modelled using an imported IFZ lattice and also via the in built matrix lattice option.
3.8	Henry's salt transport.	Steady state groundwater flow. Density dependent on salinity. Two variants are modelled, the first modelling the transport of salinity and the second using an imported density field.

Table 3-1 DFN verification tests

3.1 3D Fracture Distributions

3.1.1 Overview

This case generates sets of random fractures using a number of commonly used distributions for length and orientation. The fractures are exported and analysed to verify that the observed distribution matches the expected values.

3.1.2 Problem Definition

Random fractures are generated in a 100 m x 100 m x 100 m cube. Six variations are considered with the following combination of properties.

Symbol	Parameter	Value
ψ	Dip angle	Uniform distribution 0-180 degrees
α	Dip direction	Uniform distribution 0-180 degrees
ω	Orientation	Uniform distribution 0-180 degrees
f_d	Fracture density	0.02
L1	Fracture side length 1	Truncated power law distribution
	Minimum	1 m
	Maximum	150 m
	Exponent	2.5, 3.0, 3.5 corresponding to variations 1-3
L2	Fracture side length 2	Truncated power law distribution
	Minimum	1 m
	Maximum	150 m
	Exponent	2.5, 3.0, 3.5 corresponding to variations 1-3

Table 3-2 Input parameters for variations 1-3

The range of exponents in Table 3-2 covers cases where large fractures dominate (exponent 2.5) and also where small fractures dominate (exponent 3.5). This is illustrated in Figure 3-1, Figure 3-2 and Figure 3-3.

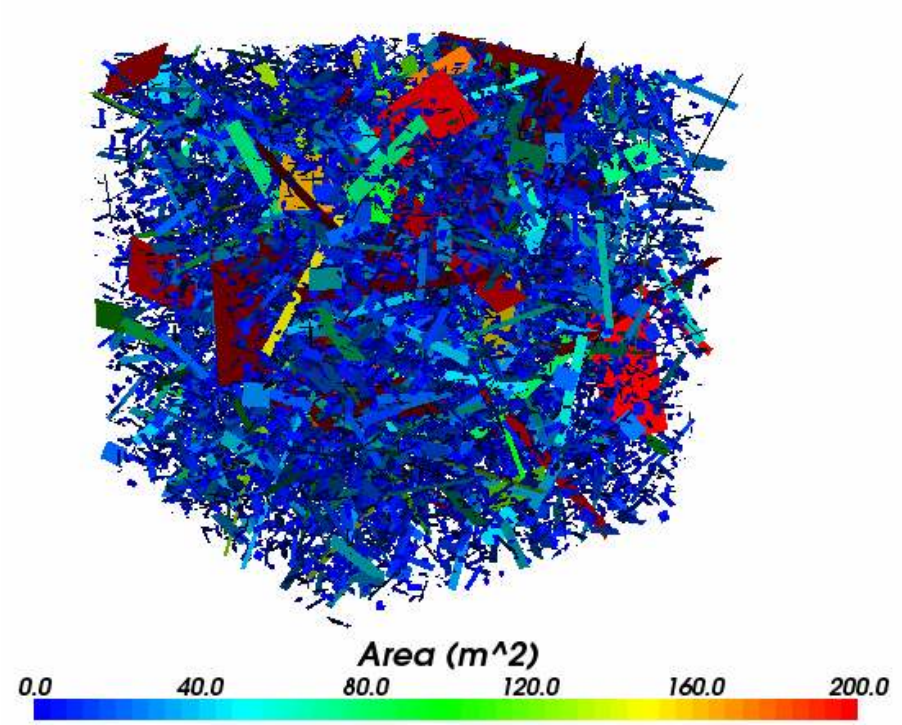

Figure 3-1 Fractures for exponent of 2.5, connectivity dominated by large fractures

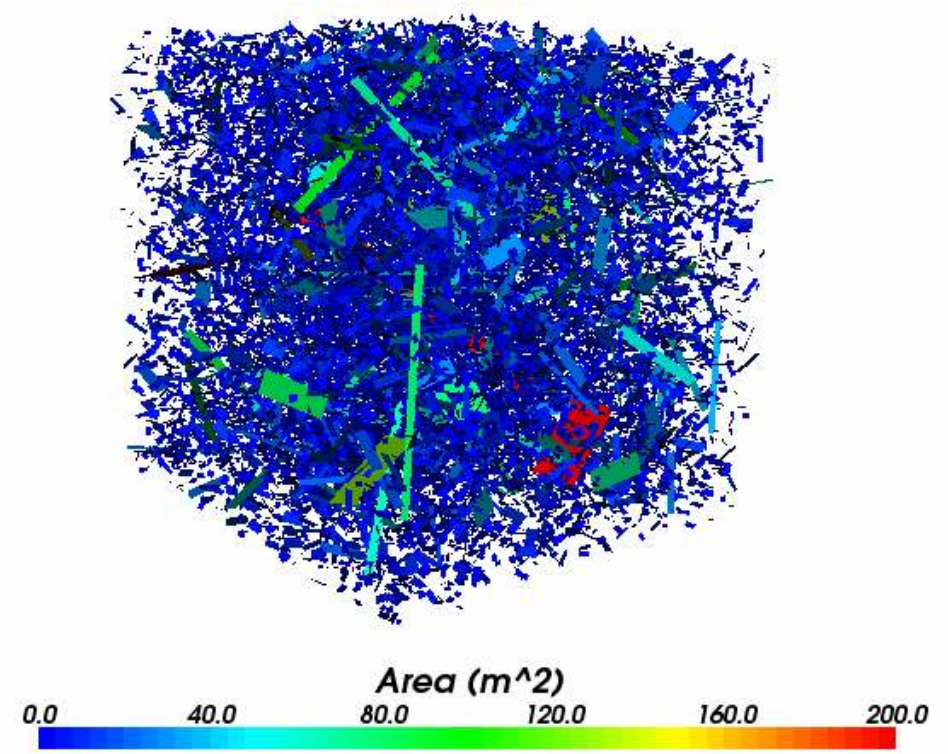

Figure 3-2 Fractures for exponent of 3.0

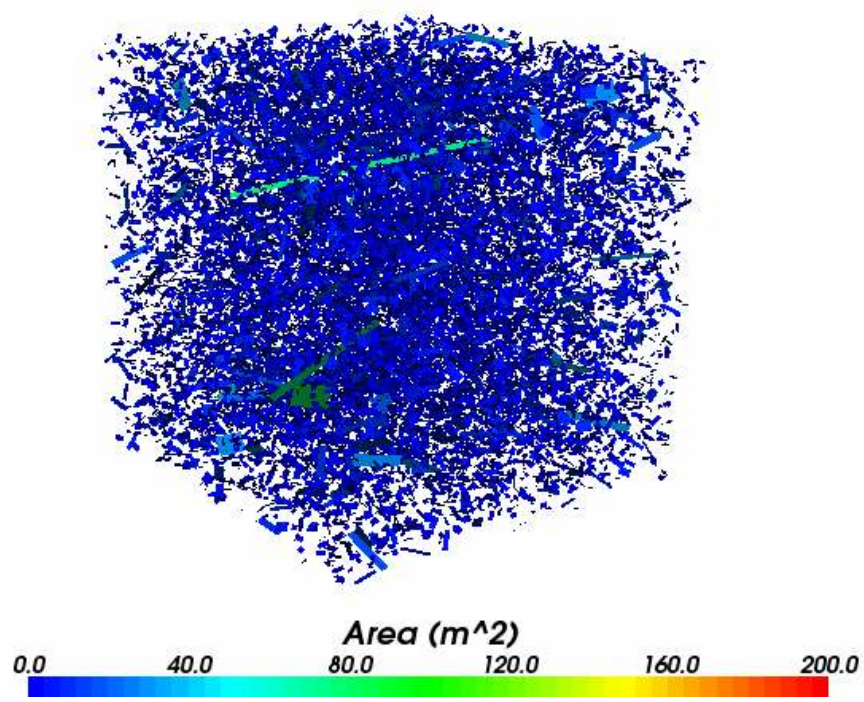

Figure 3-3 Fractures for exponent of 3.5, connectivity dominated by small fractures

Symbol	Parameter	Value
ψ	Dip angle	Fisher distribution with dispersion 5.0, 20.0, 100.0 corresponding to variations 4-6
α	Dip direction	Uniform distribution 0-180 degrees
ω	Orientation	Uniform distribution 0-180 degrees
f_d	Fracture density	0.02
L	Fracture side length of square fractures	Log normal distribution
	Mean of log(length)	2
	Standard deviation of log(length).	0.2, 0.4, 0.6 corresponding to variations 4-6

Table 3-3 Input parameters for variations 4-6

As the fisher parameter increases in variations 4-6, the fractures become increasingly parallel. At the same time the standard deviation of the log of the length is increasing in the log normal distribution which gives rise to an increased number of larger fractures. This is illustrated in Figure 3-4, Figure 3-5 and Figure 3-6.

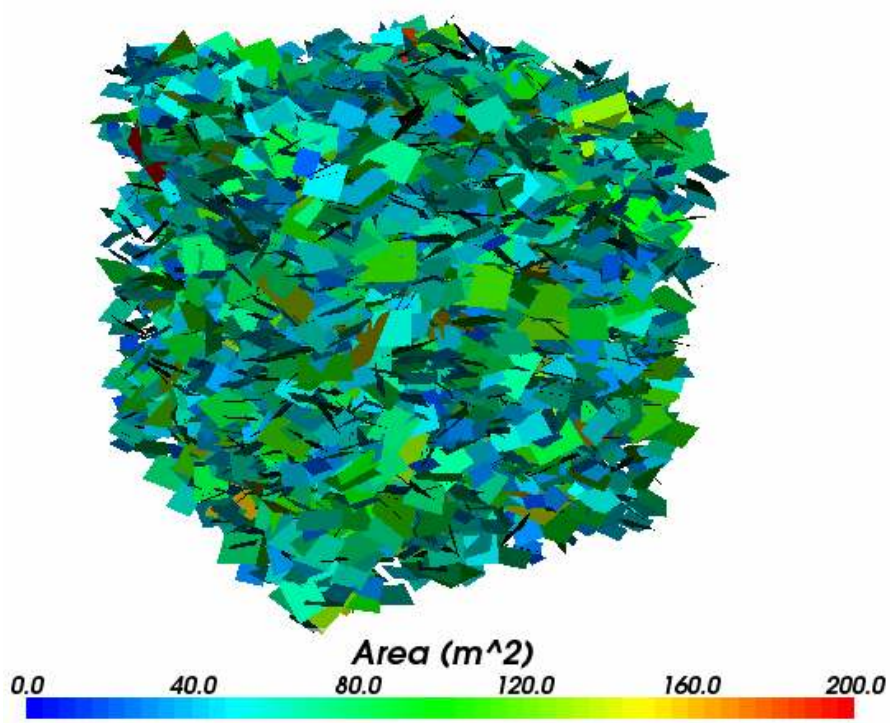

Figure 3-4 Fractures for fisher dispersion 5.0

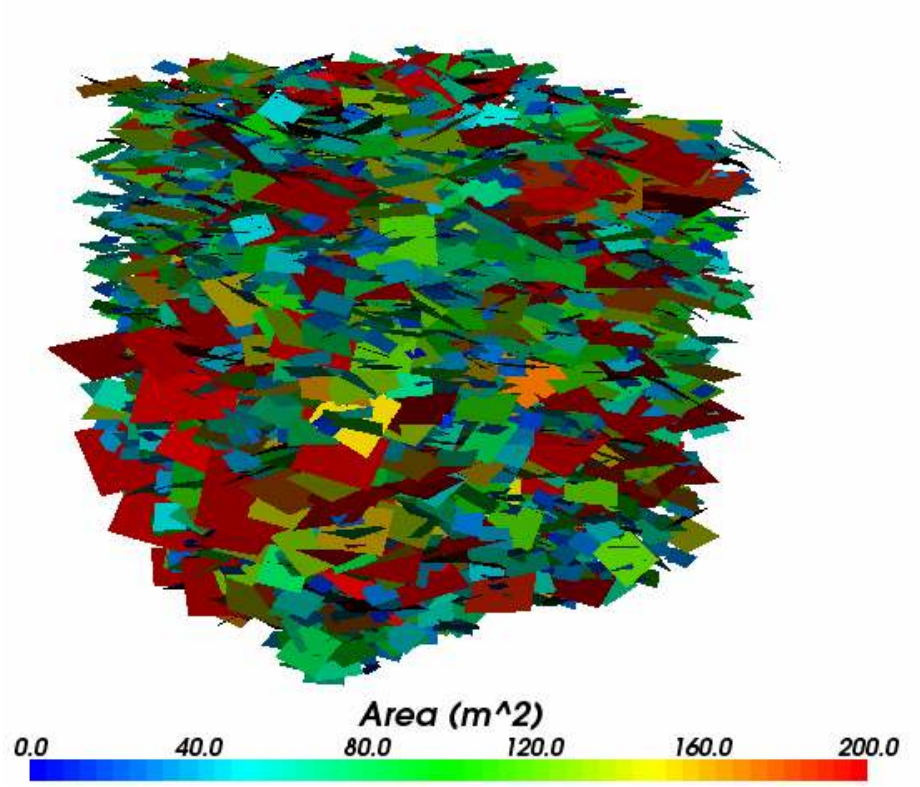

Figure 3-5 Reduced range of angles for fisher dispersion 20.0

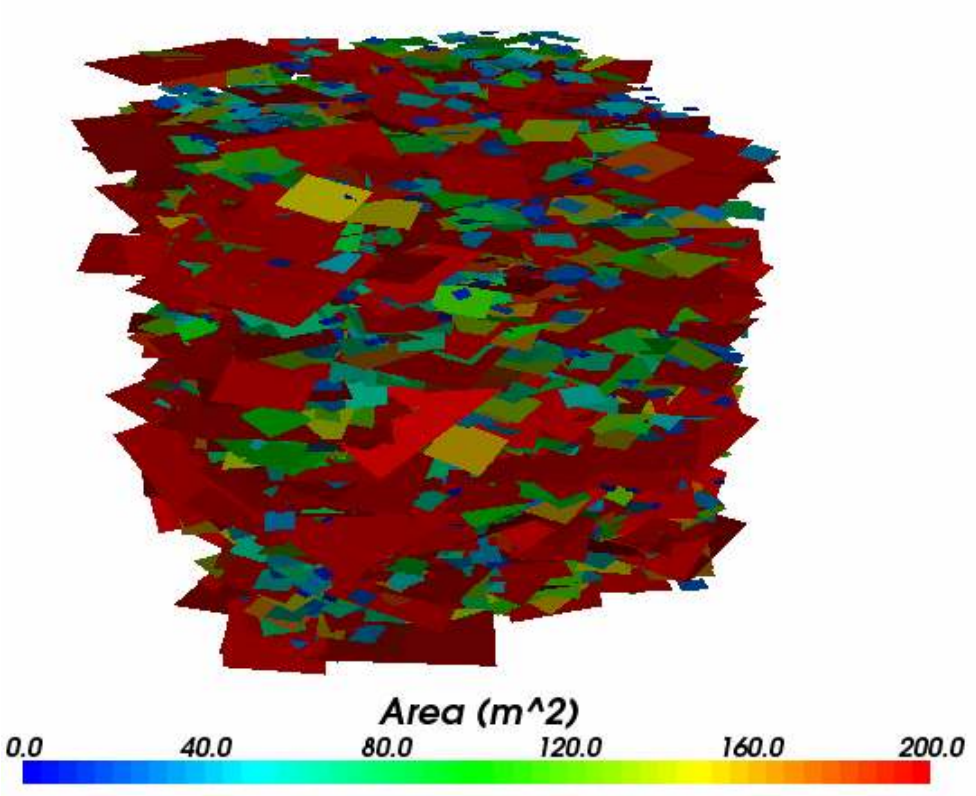

Figure 3-6 Reduced range of angles for fisher dispersion 100.0 and larger fractures due to increased standard deviation in log normal distribution.

3.1.3 Results

All results agree to within 5% of the expected values.

3.1.3.1 Variations 1-3

The volume of the region is 1.0E6 m^3, given a point density of 0.02 the expected number of generated fractures is 20000. The results for variations 1-3 are shown in Table 3-4.

Variation	Expected Value	Measured Value	Error
Variation 1	20000	19743	1.29%
Variation 2	20000	20116	0.58%
Variation 3	20000	20015	0.08%

Table 3-4 Number of randomly generated fractures

In each of these variations the fracture normal is uniformly distributed over all possible directions. This is tested by calculating the average unit normal vectors over all fractures. The magnitude of the resulting vector should approach zero as the number of fractures increases (a value of 1 would correspond to all fractures being parallel). The results for variations 1-3 are shown in Table 3-5.

Variation	Expected Value	Measured Value	Error
Variation 1	0.0	0.0031	0.31%
Variation 2	0.0	0.0095	0.95%
Variation 3	0.0	0.0065	0.65%

Table 3-5 Magnitude of Average Fracture Normal

For a set of n fractures of side length l_i and minimum side length $l_{\min}$ an estimate for the power law distribution exponent η is given in [13] as

$$\eta = 1 + n\left[\sum_{i=1}^{n} \ln\left(\frac{l_i}{l_{\min}}\right)\right]^{-1}$$

Applying this to variations 1-3, gives the results shown in Table 3-6 and Table 3-7.

Variation	Expected Value	Measured Value	Error
Variation 1	2.5	2.513	0.52%
Variation 2	3.0	3.035	1.16%
Variation 3	3.5	3.510	0.29%

Table 3-6 Estimated power law exponent for fracture side length 1

Variation	Expected Value	Measured Value	Error
Variation 1	2.5	2.513	0.52%
Variation 2	3.0	3.017	0.57%
Variation 3	3.5	3.514	0.40%

Table 3-7 Estimated power law exponent for fracture side length 2

3.1.3.2 Variations 4-6

The volume of the region is 1.0E6 m^3. Given a point density of 0.02, the expected number of generated fractures is 20000. The results for variations 4-6 are shown in Table 3-8.

Variation	Expected Value	Measured Value	Error
Variation 4	20000	19740	1.30%
Variation 5	20000	19896	0.52%
Variation 6	20000	19771	1.15%

Table 3-8 Number of randomly generated fractures

For a set of n fractures with angle θ to the average normal, an estimate for the fisher dispersion parameter κ is given in [14] as

$$\kappa = \frac{R(3-R^2)}{1-R^2} \text{ where } R = \frac{1}{n}\sum_{i=1}^{n} \cos(\theta)$$

Applying this to variations 4-6, gives the results shown in Table 3-9

Variation	Expected Value	Measured Value	Error
Variation 4	5.0	5.14	2.90%
Variation 5	20.0	20.11	0.55%
Variation 6	100.0	100.06	0.06%

Table 3-9 Fisher distribution parameter

For a log normal distribution, the arithmetic mean and standard deviation are given in [15] as

$$\mu = e^{\mu_l + \frac{\sigma_l^2}{2}} \text{ and } \sigma = e^{\mu_l + \frac{\sigma_l^2}{2}} \sqrt{e^{\sigma_l^2} - 1}$$

Where μ_l and σ_l are the mean and standard deviation of the log of the distribution. Applying this to the fracture length distribution in variations 4-6 gives the results shown in Table 3-10 and Table 3-11.

Variation	Expected Value	Measured Value	Error
Variation 4	7.53	7.48	0.68%
Variation 5	8.00	7.96	0.62%
Variation 6	8.85	8.73	1.29%

Table 3-10 Average side length for log normal distribution

Variation	Expected Value	Measured Value	Error
Variation 4	1.52	1.54	1.17%
Variation 5	3.33	3.29	1.20%
Variation 6	5.82	5.59	3.92%

Table 3-11 Standard deviation of side length for log normal distribution

3.2 3D Fracture Connectivity

3.2.1 Overview

The DFN software has the ability to create networks of random fractures with specified properties. This case uses percolation theory to check the generation and connectivity of random fractures within a cube.

3.2.2 Problem Definition

The modelled domain is a cube of side length 20 m. This is filled with randomly generated square fractures with side length 1 m and with random orientation and position. This is illustrated in Figure 3-7.

Symbol	Parameter	Value
ψ	Dip angle	Uniform distribution 0-90 degrees
α	Dip direction	Uniform distribution 0-90 degrees
ω	Orientation	Uniform distribution 0-90 degrees
l	Fracture side length	1 m
L	Cube side length	20 m

Table 3-12 Input parameters

The critical areal density at which all surfaces of the cube should be connected by the fracture network is given in [16] as 1.23.

3.2.3 Results

Thirty different random numbers seeds were used. For each seed a progression of areal densities were used in order to estimate the critical density. The average resulting critical density was 1.32, 7.3% higher than in [16].

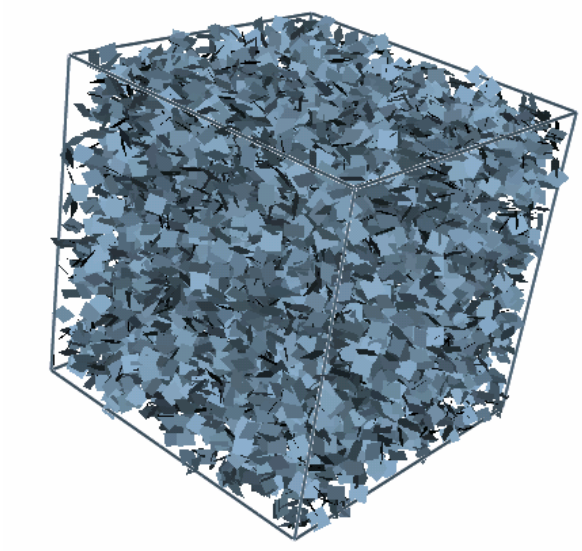

Figure 3-7 Fractures at critical areal density

3.3 3D Fracture Connectivity with a Power Law Size Distribution

3.3.1 Overview

This case considers the connectivity of random fractures within a cube, where the fracture lengths follow a power law distribution. The solution is taken from [17].

3.3.2 Problem Definition

The modelled domain is a cube for a range of increasing sizes. This is filled with randomly generated square fractures with side length corresponding to a truncated power law.

Symbol	Parameter	Value
ψ	Dip angle	Uniform distribution 0-90 degrees
α	Dip direction	Uniform distribution 0-90 degrees
ω	Orientation	Uniform distribution 0-90 degrees
a	Exponent in power law	2.5
L	Cube side length	5 - 300 m

Table 3-13 Input parameters

When the exponent is less than 3 the critical fracture density varies with domain size and the connectivity is dominated by the larger fractures. This is illustrated in Figure 3-9.

For large values of the exponent the connectivity of the smaller fractures dominates and the critical density does not vary with domain size for sufficiently large domains. This is similar to case 0

3.3.3 Results

A comparison of the dependence of the critical density on domain size is shown in Figure 3-8. The reference data is taken from [16].

The results from ConnectFlow show good agreement, particularly in terms of the slope which, as discussed in [16], varies significantly with the exponent a.

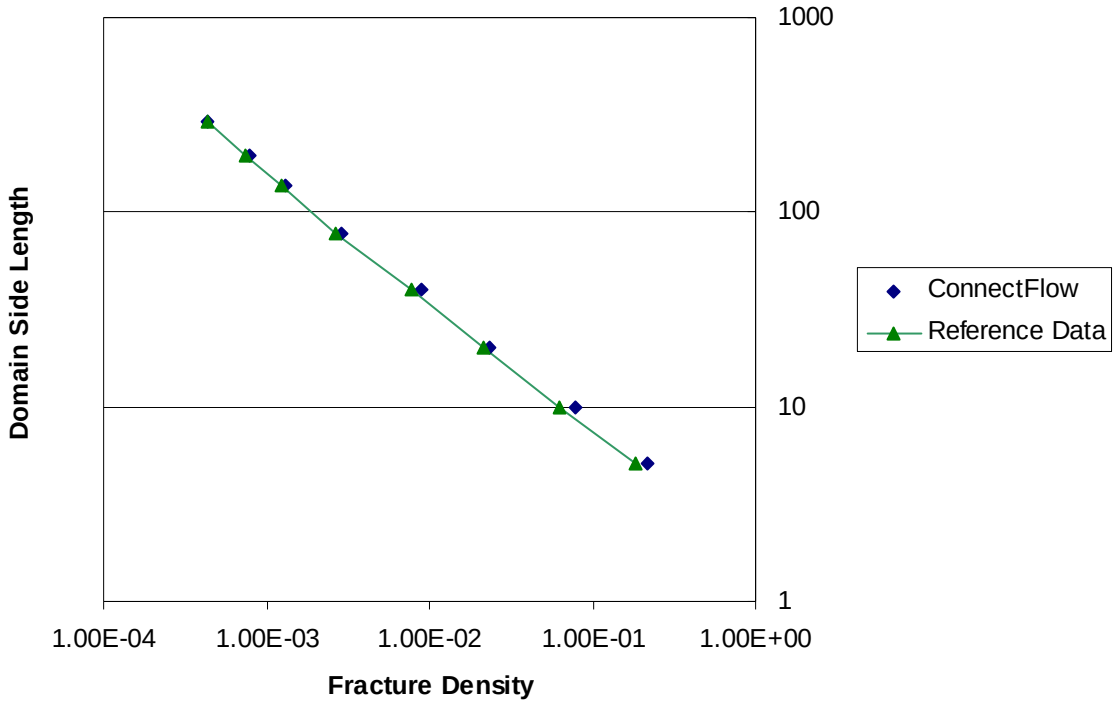

Figure 3-8 Critical fracture density variation with domain size

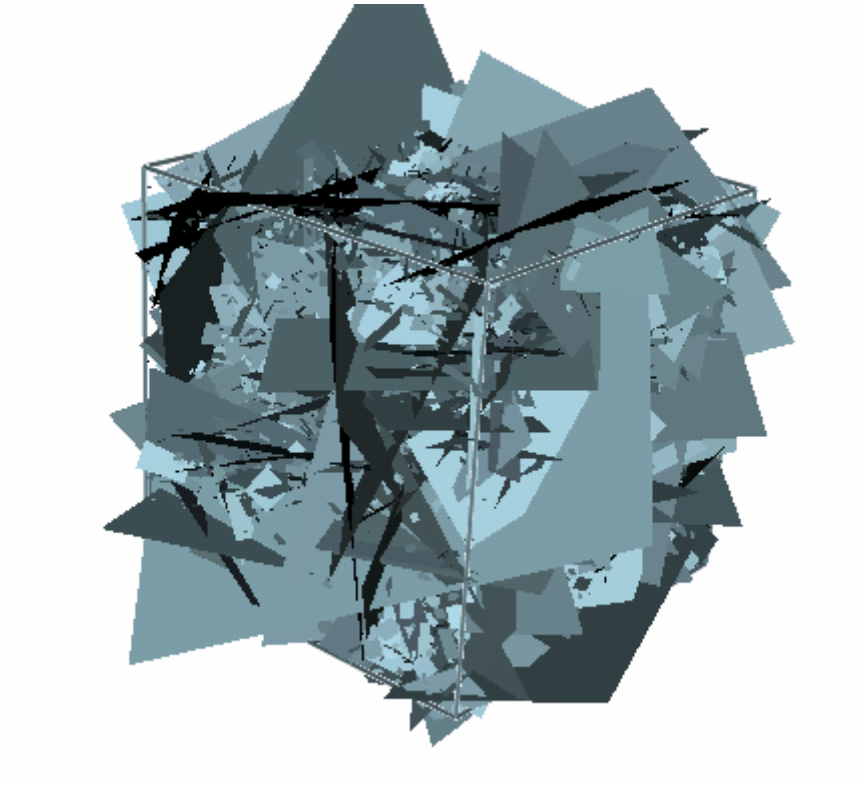

Figure 3-9 Fracture network generated using a power law size distribution (a=2.5)

3.4 Upscaling from DFN to CPM

3.4.1 Overview

This case is taken from the DECOVALEX Task C [18] and calculates the permeability through a 20 m x 20 m region of fractured rock, generated from fracture mapping data from Sellafield UK.

The fracture set consists of 7797 fractures, with lengths varying from 0.5 to >30 m, and apertures varying from 1 to 200 microns.

The upscaled permeabilties are then used in a CPM calculation and the mass flows are compared.

3.4.2 Problem Definition

The modelled domain consists of a 20 m x 20 m x 1 m region with an applied horizontal pressure gradient of 1.0E4 Pa/m, as illustrated in Figure 3-10.

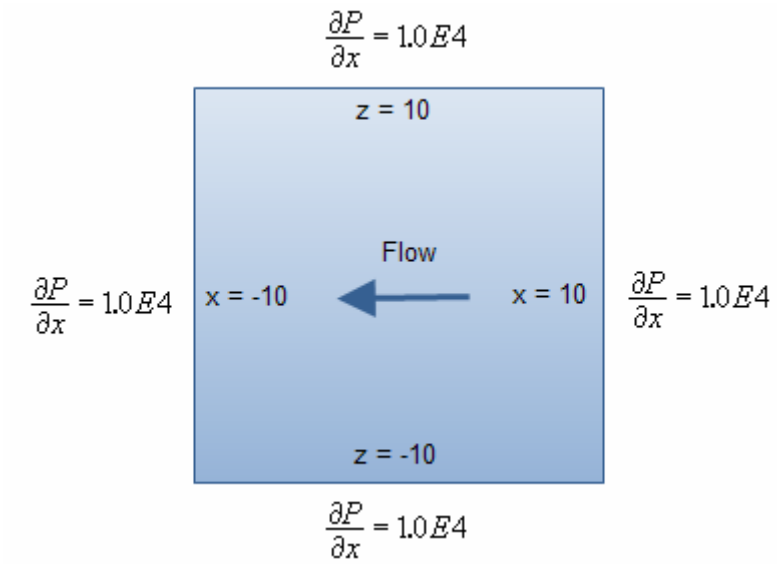

Figure 3-10 Schematic of problem definition

The fracture distribution is shown in Figure 3-11 and the input parameters in Table 3-14.

Symbol	Parameter	Value
ρ	Density	1000 kg/m^3
μ	Viscosity	1.0E-3 Ns/m^2

Table 3-14 Input parameters

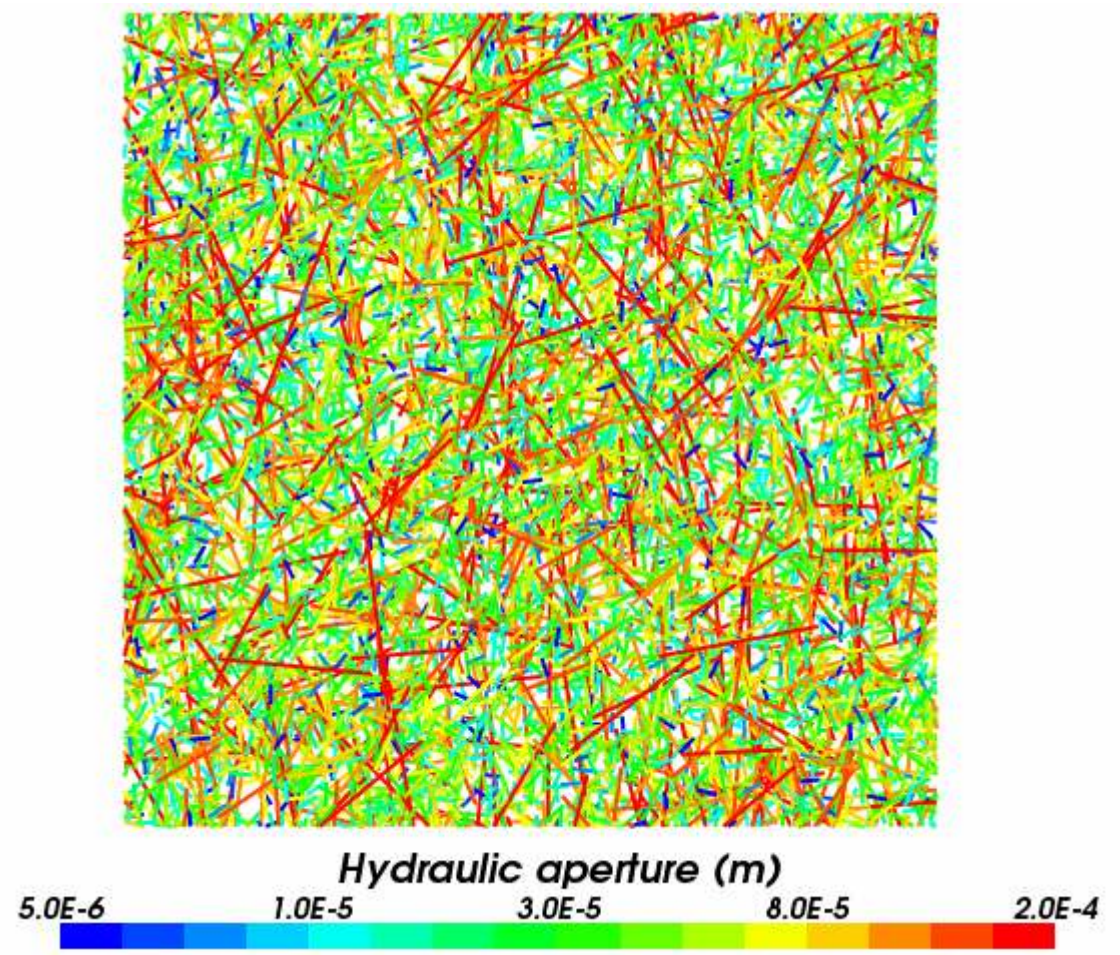

Figure 3-11 Fractured Rock

The DFN permeabilities are calculated on a regular grid of cells and the CPM calculation uses a regular grid of the same resolution. The finest grid resolution tested was 400x400 cells.

3.4.3 Variations

3.4.3.1 Cellular Model Calculation

The DFN region is overlayed with a grid of cells of the required resolution. This is used for all results except Figure 3-14.

3.4.3.2 Cellular Model with Guard Zone

Each cell is stretched by a factor 3 in the x and z directions and then the middle section is used to export permeabilities for the area of interest. This helps improve accuracy where single fractures intersect more than one of the cells sides.

3.4.3.3 Regional Model Calculation

The DFN model region is used to define the grid of cells.

3.4.4 Results

The overall flow through the left hand boundary x=-10 is compared against the stress free TUL results from [18] and the upscaled NAMMU results. All results agree to within 6%.

Approach	Flow X=-10
TUL	9.40E-5 m^3/s
ConnectFlow DFN	9.62E-5 m^3/s
ConnectFlow CPM (400 x 400 upscaling)	9.96E-5 m^3/s

The distribution of outflow at x = -10 m is compared between NAPSAC and NAMMU in Figure 3-12 for a range of upscaling resolutions. The data is averaged over 1 m intervals in order to better compare the bulk profile. Flow orthogonal to the pressure gradient at the outflow boundary z = 10 m is shown in Figure 3-13.

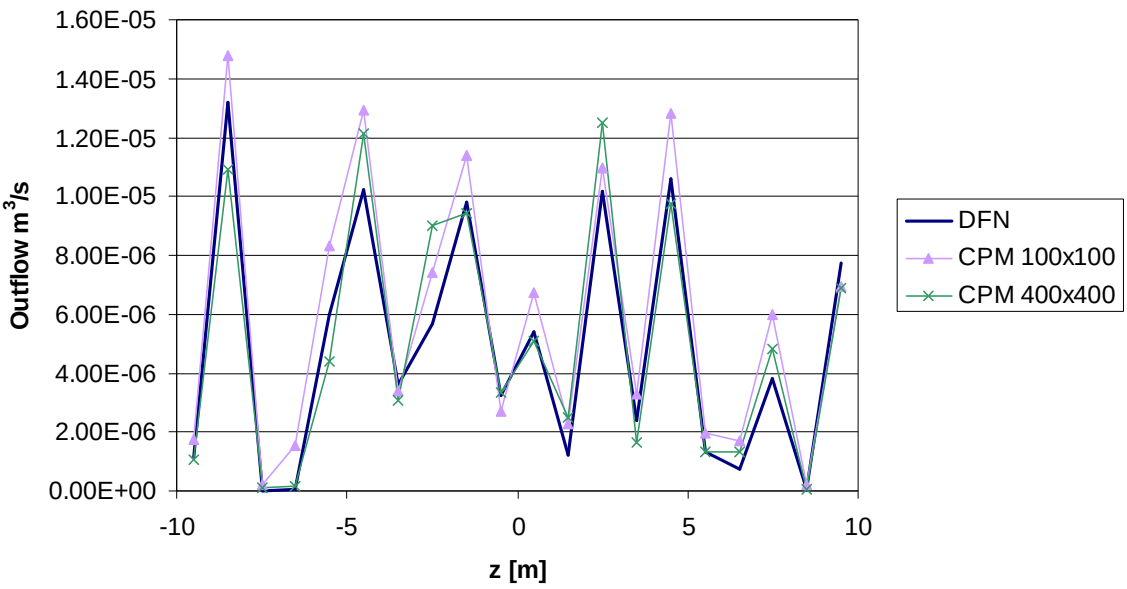

Figure 3-12 Outflow distribution at left boundary (X=-10 m) for cellular model upscaling with no guard zone

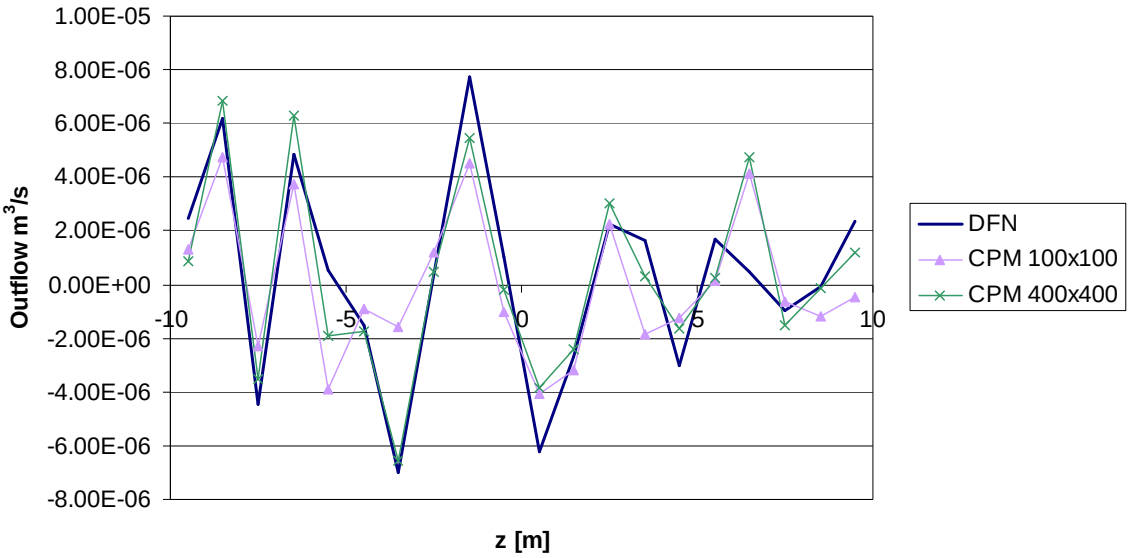

Figure 3-13 Outflow distribution at top boundary (Z=10 m) for cellular model upscaling with no guard zone

The overall outflow through the 20 m top surface is 5.45E-6 m3/s as computed by the DFN model and 6.01E-6 m3/s as computed by the CPM 400x400 model. This is around 1/20th of the outflow in the direction aligned with the pressure gradient.

Figure 3-14 compares the outflow distribution across the three variations in 3.4.3 for an upscaling resolution of 100x100. The Cellular and Model Region variations are virtually identical as expected. Use of the guard zone improves the agreement as compared with the DFN solution.

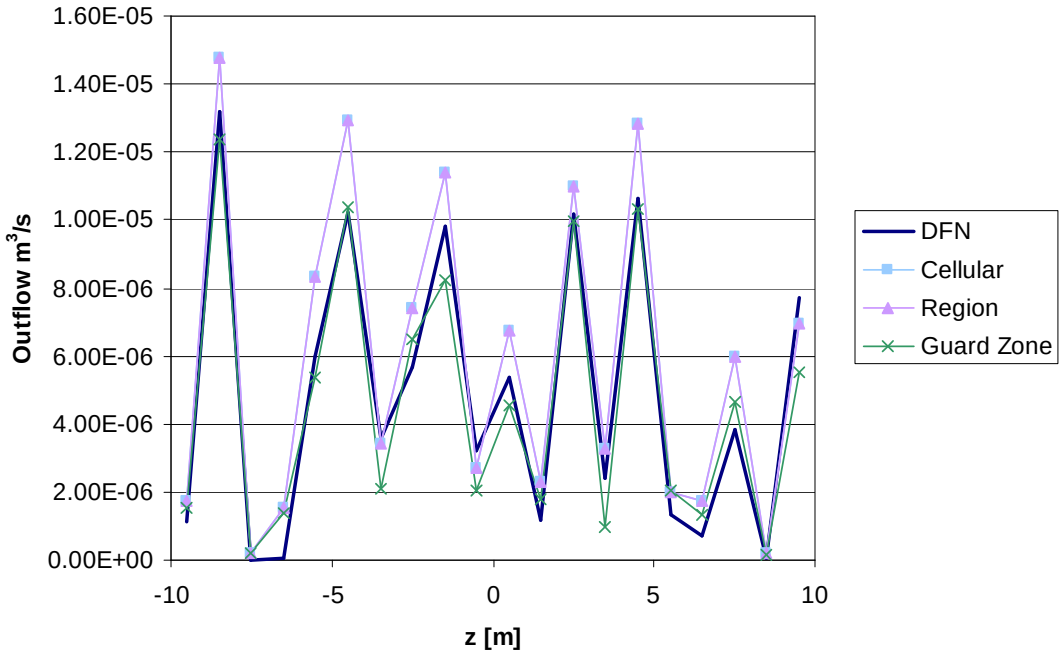

Figure 3-14 Comparison of outflows at left boundary (X=-10m) using a CPM resolution of 100x100

3.5 Radial Steady State Flow

3.5.1 Overview

This case models steady groundwater flow in a 2D disk where water is removed from the centre at a constant rate and the outer disk boundary is maintained at a constant head.

The example has a simple analytical solution and can be used to test a range of modelling choices.

3.5.2 Problem Definition

This case is the DFN equivalent of case 0.

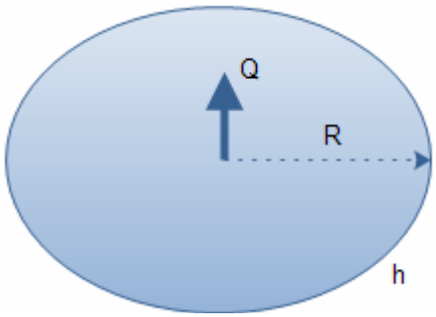

Figure 3-15 Schematic of problem definition

For a fracture, the aperture, *e*, is related to the hydraulic conductivity, *K* by

$$e = \sqrt{\frac{12K\mu}{\rho g}}$$

The values in Table 3-15 have scaled Q from 1.0E-7 in case 0 to give an equivalent head distribution.

A 5 degree sector of the disk is modelled and is tessellated using 100 single fractures along its length. As these fractures are not rectangular, ConnectFlow breaks them up into right angle triangles as illustrated in Figure 3-16.

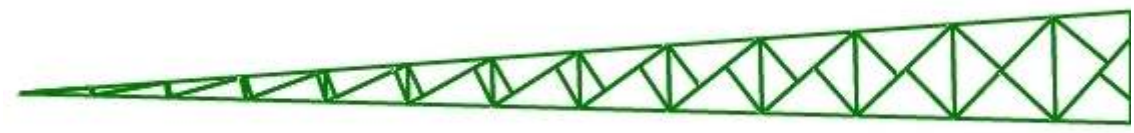

Figure 3-16 Fractures in sector of disk

The fractures used model the circumference of the sector as a straight line. As a result the accuracy of the simulation increases as the angle of the sector decreases.

The outflow at the axis is modelled using a borehole with a specified flow rate which has direction orthogonal to the disk.

Symbol	Parameter	Value
h	Head at disk circumference	0 m
Q	Outflow from disk	1.11E-14 m^3/s
K	Hydraulic Conductivity	1.0E-8 m/s
R	Radius of disk	2000 m
e	Aperture of fracture	1.11E-7 m
r	Radial distance from axis	0-2000 m
ρ	Density	1000 kg/m^3
μ	Viscosity	1.0E-3 Pa.s
g	Gravity	9.8 m/s^2

Table 3-15 Input parameters

3.5.3 Results

The analytical solution is given by

$$h(r) = h(R) - \frac{Q}{2\pi Kd}\ln(\frac{R}{r})$$

The results from ConnectFlow show good agreement with the analytical solution, as illustrated in Figure 3-17.

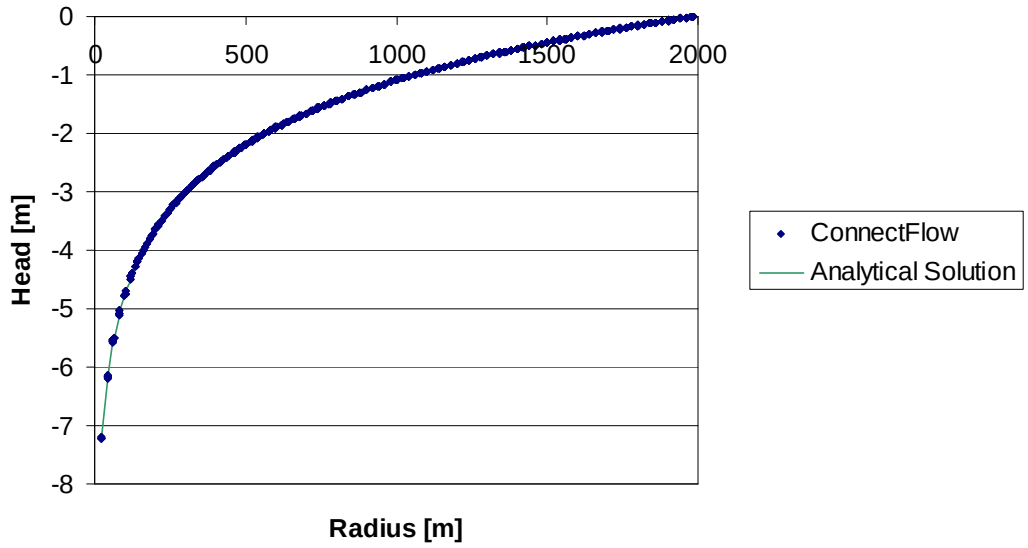

Figure 3-17 Variation of head with distance from the axis with an outflow modelled with a borehole

3.6 Three Fracture Intersections

3.6.1 Overview

This case models steady groundwater flow and particle tracking in a simple two dimensional fracture network.

3.6.2 Problem Definition

The problem is a variant of test C1 from DarcyTools [19]. Three fractures are placed in a rectangular region as shown in Figure 3-18.

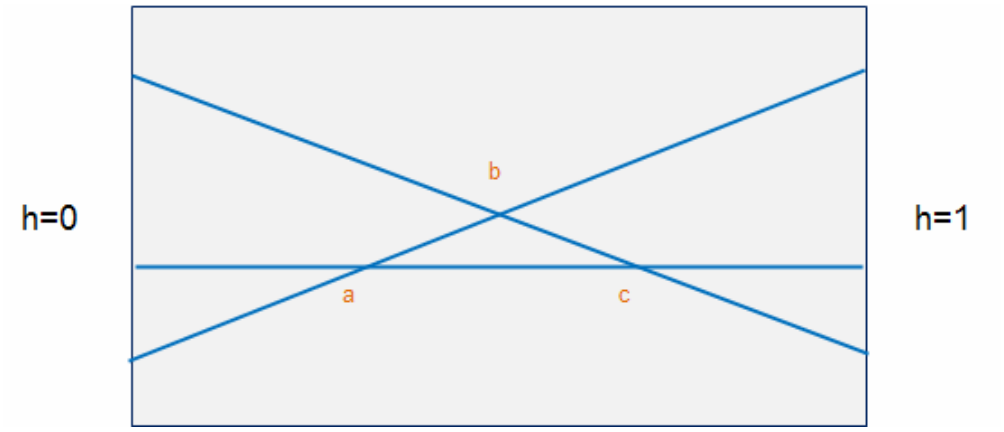

Figure 3-18 Three fracture intersections

A 3x3 system of linear equations is derived by applying mass conservation at the three fracture intersections. This is used to calculate the heads at a, b and c and hence the flow rates in each fracture segment.

The fracture geometry used for this test is defined in Table 3-16.

X Start	Y Start	X End	Y End
0	2	12	5
0	3	12	3
0	5	12	2

Table 3-16 Fracture locations

3.6.3 Variations

3.6.3.1 Symmetric

For the symmetric case, the fracture aperture is set to 1.0E-4 m for all three fractures. This gives an analytical flow field where the flow rates along each fracture are almost identical.

3.6.3.2 Non-symmetric

In the non-symmetric case, the fracture apertures are set to 1.0E-4 m for the fracture passing through section bc, 2.0E-4 m for section ac and 4.0E-4 m for section ab. In addition, the section of fracture passing through ab is removed as shown in Figure 3-19.

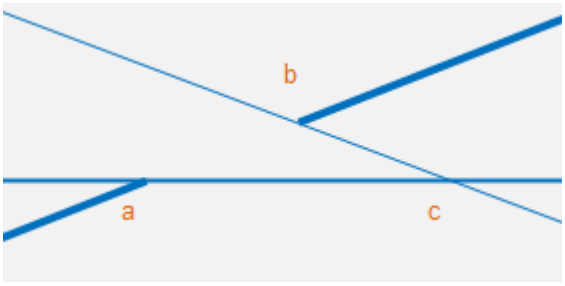

Figure 3-19 Non symmetric fractures

This arrangement means that the flow at b splits, with some of it moving to c and then a, and the rest moving directly towards the left hand boundary.

The particle tracking is tested by releasing 10000 particles at the h=1 surface, with the fraction of particles in each fracture distributed in proportion to the analytical inflow rate.

The proportion of particles leaving the geometry at Y=2, 3 and 5 should correspond to the ratio of the analytically predicted outflow rates.

Y	Analytical inflow distribution at X=12	Analytical outflow distribution at X=0
2	7.9%	77.3%
3	64.9%	10.0%
5	27.2%	12.7%

Table 3-17 Analytical inflow/outflow

For this test, the `APPROXIMATE PARTICLE TRACKING` model is used, with forward tracking to track from inflow to outflow and backward tracking to track from outflow to inflow.

3.6.4 Results

3.6.4.1 Symmetric

The predicted results for head are within 1% of the analytical values.

Intersection	ConnectFlow	Analytical	% Error
a	0.333	0.333	0.19%
b	0.496	0.500	0.89%
c	0.667	0.667	0.10%

Table 3-18 Heads at fracture intersections

3.6.4.2 Non Symmetric

The ConnectFlow head distribution for this case is shown in Figure 3-20. Predicted results for the head and particle flows are within 5% of the analytical values.

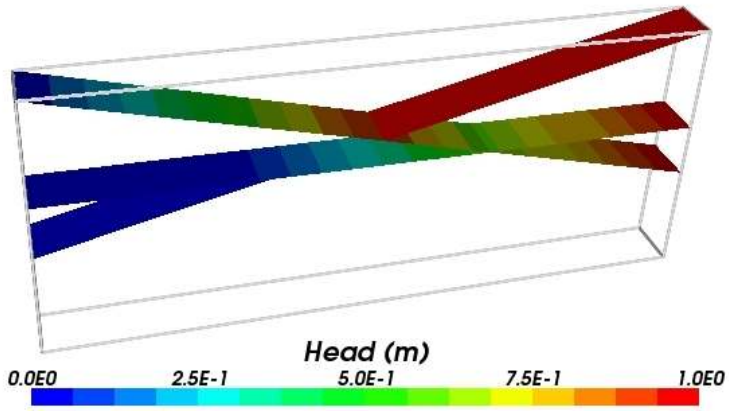

Figure 3-20 Head distribution

Intersection	ConnectFlow	Analytical	% Error
a	0.062	0.061	1.49%
b	0.937	0.968	3.23%
c	0.599	0.600	0.15%

Table 3-19 Heads at fracture intersections

Y at Exit	ConnectFlow	Analytical	Error
2	7.4%	7.9%	0.5%
3	65.6%	65.0%	0.6%
5	27.0%	27.2%	0.2%

Table 3-20 Particle flow rates (Backwards)

Y at Exit	ConnectFlow	Analytical	Error
2	77.6%	77.3%	0.3%
3	9.5%	10.0%	0.5%
5	12.9%	12.7%	0.2%

Table 3-21 Particle flow rates (forwards)

3.7 Steady Flow in Fractured Rock

3.7.1 Overview

The example is taken from Level 1 of the international HYDROCOIN project for verification of groundwater flow codes [20] and is the same problem as CPM case 2.2.

It models steady state flow in a two-dimensional vertical slice of fractured rock. The rock contains two inclined fractures which intersect one another at depth, and have a higher permeability than the surrounding rock.

The topography has been made simple so that it consists of two valleys located where the fracture zones meet the surface. To simplify the problem definition, the shape of the surface is described by straight lines. Although the surface topography is symmetric, the flow is influenced by the asymmetry of the fracture zones.

This problem is based on an idealized version of the hydrogeological conditions encountered at a potential site for a deep repository in Swedish bedrock. A detailed three-dimensional model of this was made in a separate study [21].

3.7.2 Problem Definition

Figure 3-21 depicts the modelled domain.

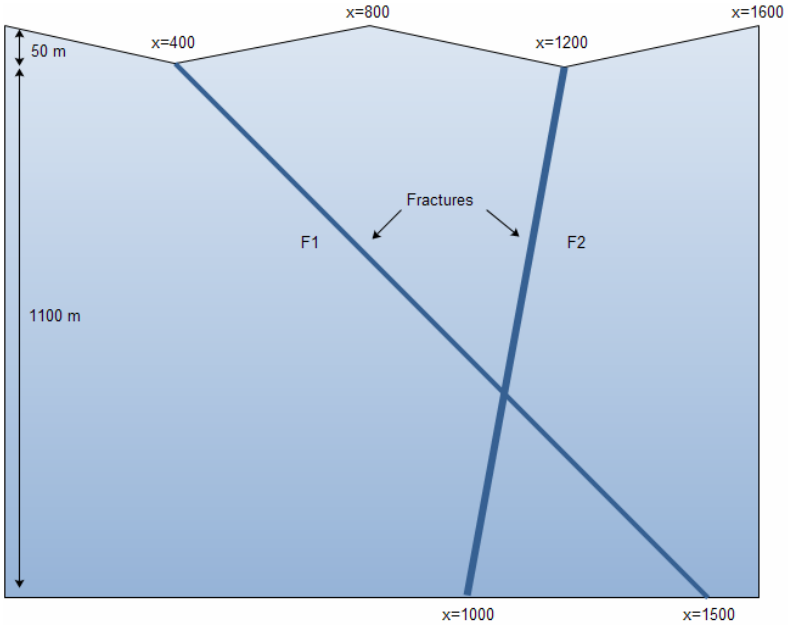

Figure 3-21 Fractured rock

Symbol	Parameter	Value
K_r	Hydraulic conductivity of rock	1.0E-8 m/s
K_{rf}	Hydraulic conductivity of CPM fractured region	1.0E-6 m/s
e_1	Thickness of fracture F1	2.053E-4 m
e_2	Thickness of fracture F2	2.620E-4 m

Table 3-22 Input parameters

The fracture apertures have been derived to match the transmissivities of the fracture regions in case 2.2.2. For the DFN model, the transmissivity is proportional to aperture cubed and for the CPM model it is proportional to the cross sectional thickness of the region representing the fracture.

The rock is modelled using an array of fractures as shown in Figure 3-22. The figure is drawn in perspective to make it easier to visualise.

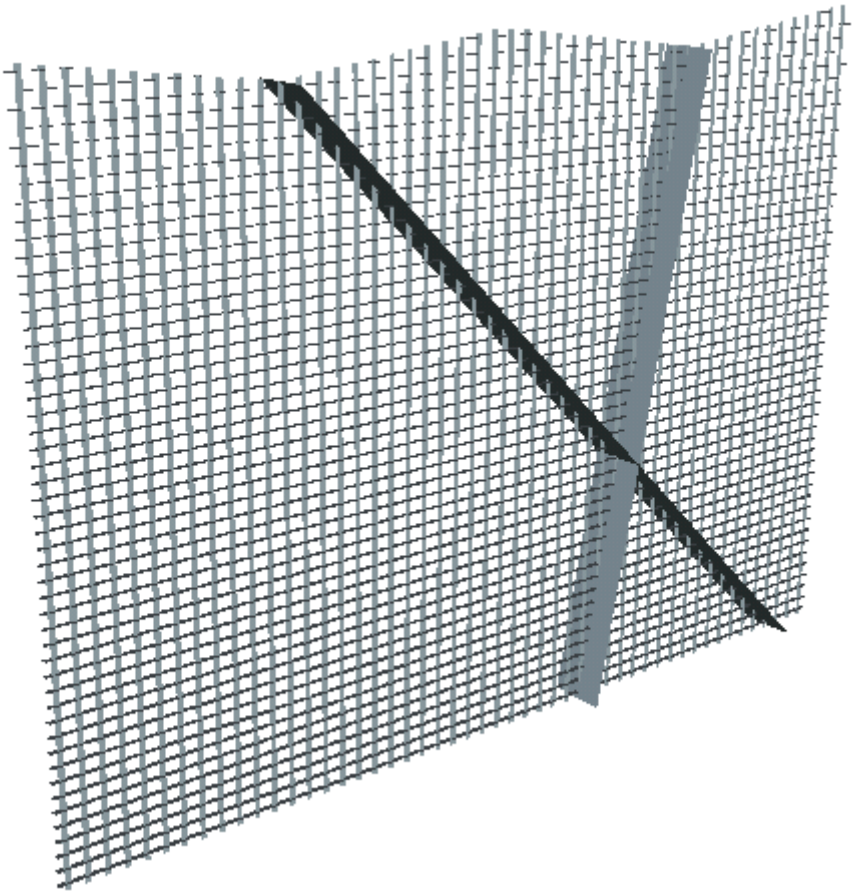

Figure 3-22 Modelled fractures

3.7.3 Variations

3.7.3.1 IFZ Rock Matrix

In this variant, the rock matrix is modelled using a two dimensional grid of fractures that are read in as an Implict Fracture Zone (IFZ) file.

3.7.3.2 Matrix Lattice Option

In this variant, the rock matrix is modelled using a three dimensional grid of fractures generated by the command `GENERATE MATRIX LATTICE.` In this case, the fracture widths are set automatically and are approximately twice as wide as that set manually in the IFZ Rock Matrix variant.

3.7.3.3 Current Value

In this variant, a subset of the domain is modelled, x = 100 to 1500 m and y = -300 to -100 m. This is illustrated in Figure 3-23.The boundary pressure is taken from the CPM solution 2.2.3.1 and

applied using the >>CURRENT VALUE boundary condition option. The rock matrix is modelled using the same IFZ approach as in 3.7.3.1.

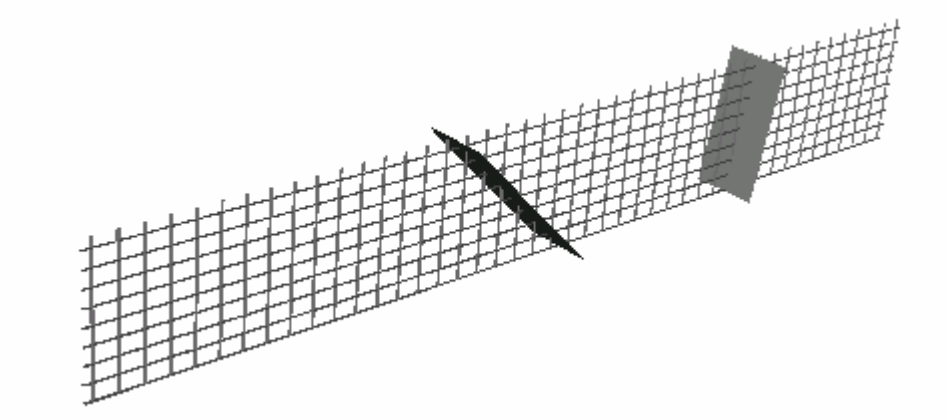

Figure 3-23 Current Value

3.7.4 Results

The results presented here compare the head profile at a height of y=-200 m and show excellent agreement with the HYDROCOIN study.

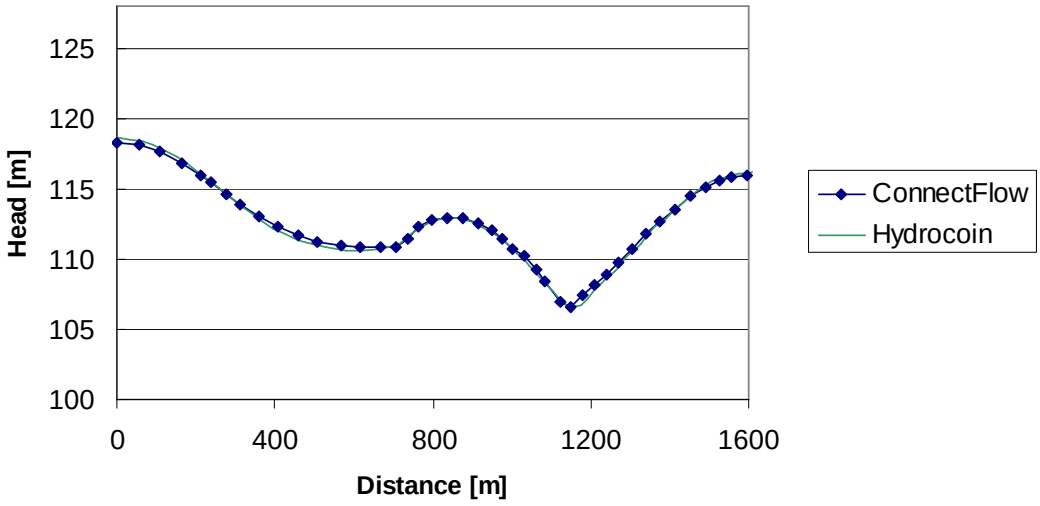

Figure 3-24 Head at height -200 m (IFZ Rock Matrix)

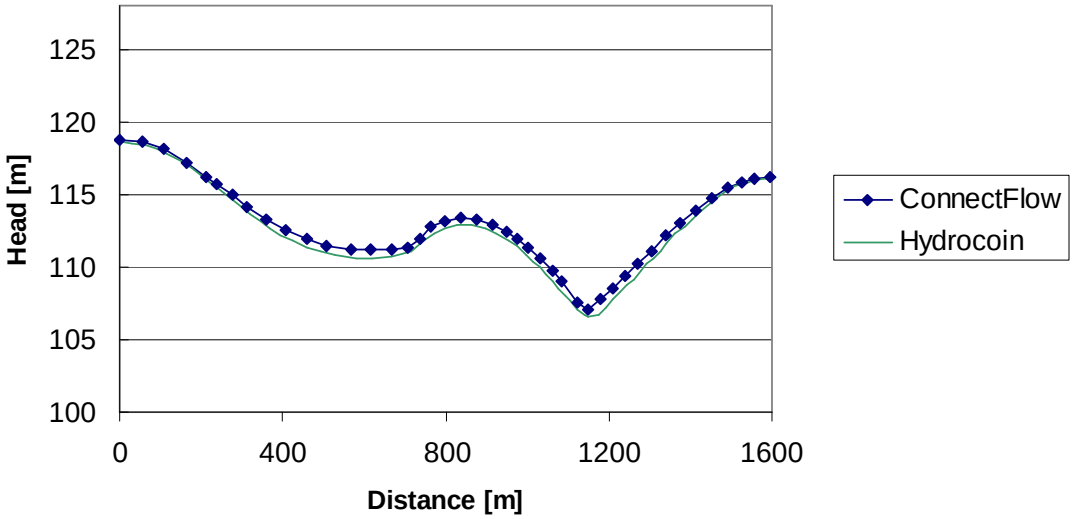

Figure 3-25 Head at height -200 m (Matrix Lattice)

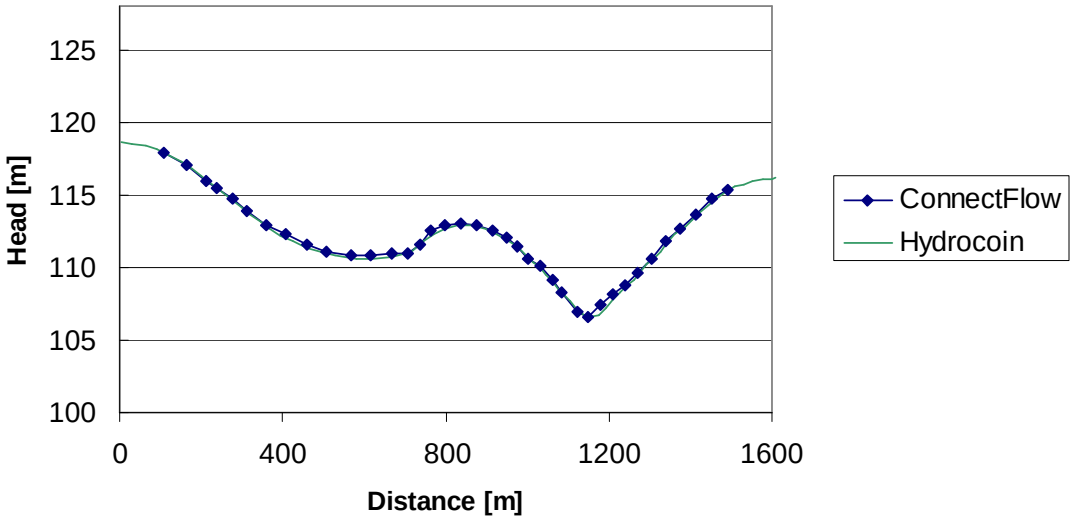

Figure 3-26 Head at height -200 m (Current Value)

In addition, the ConnectFlow results were compared against the Feftra base case results [3], with the differences in head between the two codes being less than 0.5% for the IFZ Rock Matrix and Reduced Domain variants and less than 1% for the Matrix Lattice.

The latter is marginally less accurate due to the increased permeability contribution of the wider rock matrix fractures. This was checked by making the fractures in the IFZ Rock Matrix variant deliberately wider and the same trend was seen.

Figure 3-27 shows the head distribution through the fracture network.

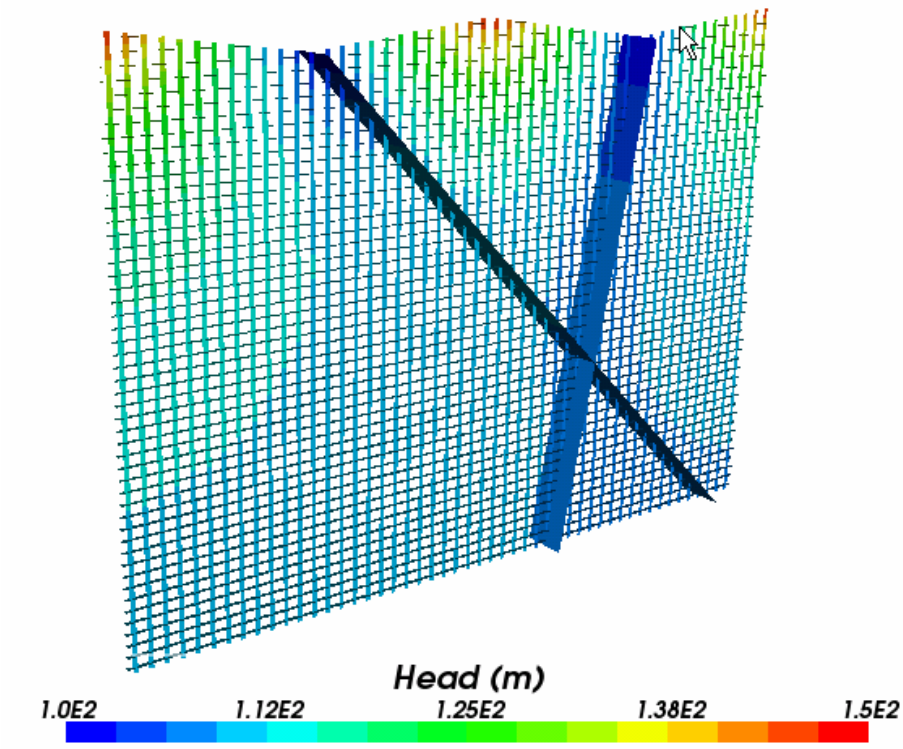

Figure 3-27 Fractures coloured by head (IFZ Rock Matrix)

3.8 Henry's Salt Transport

3.8.1 Overview

This case considers salt water intrusion into a vertical slice of an isotropic homogeneous confined aquifer.

The variant modelled is a modified version of the original Henry's test case, as recommended in [9]. The modified case halves the fresh water inflow rate, which increases the sensitivity of the solution to the variation in density.

This case is the DFN equivalent of case 2.6.

3.8.2 Problem Definition

A schematic of the test case is shown in Figure 3-28 and the input parameters are given in Table 3-23.

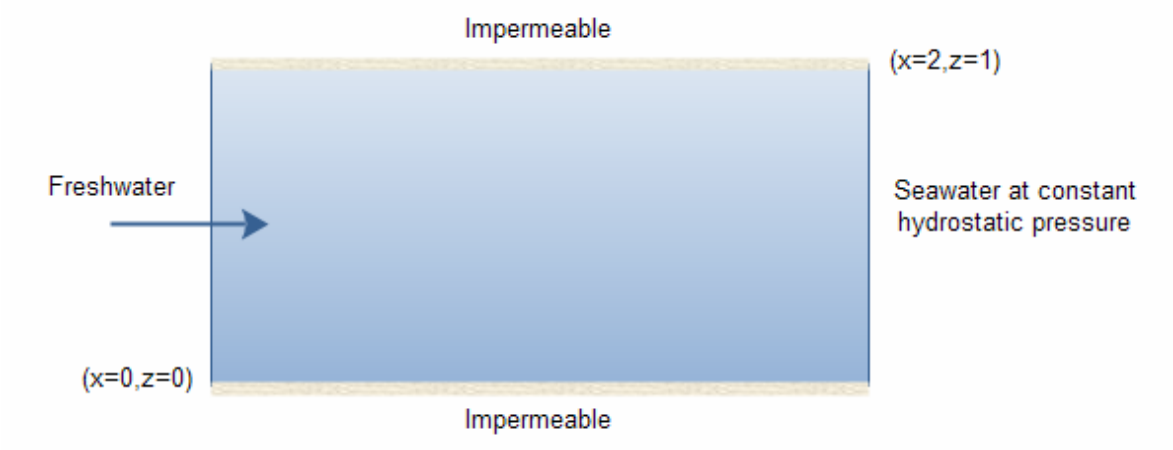

Figure 3-28 Schematic illustration of the Henry test case

Symbol	Parameter	Value
K	Hydraulic conductivity of rock	1.0E-2 m/s
D	Coefficient of molecular diffusion	1.886E-5 m^2/s
Q	Freshwater inflow per unit depth	9.43E-5 m^2/s
ρ_0	Reference density	998 kg/m^3
ρ_{max}	Saltwater density	1023 kg/m^3
α_L	Longitudinal dispersivity	0 m
α_T	Transverse dispersivity	0 m
ϕ	Porosity	1

Table 3-23 Input parameters

The domain is represented by a single fracture tessellated into 0.025 m square sub-fractures. The fracture thickness is set to 1.8516E-4 m in order to generate the desired hydraulic conductivity of 1.0E-2 m/s.

The fracture has a porosity of 1.0 rather than 0.35 in [9]. The inflow rate is increased by a factor of 1/0.35 in order to account for this and to get the appropriate velocity field.

3.8.3 Variations

3.8.3.1 Interpolated Density

The density is interpolated from the CPM solution of test case 2.6 and kept fixed throughout the calculation.

3.8.3.2 Salt Transport

The salt transport is modelled and the density calculated from the salinity.

3.8.4 Results

3.8.4.1 Interpolated Density

The interpolated density field used is shown in Figure 3-29.

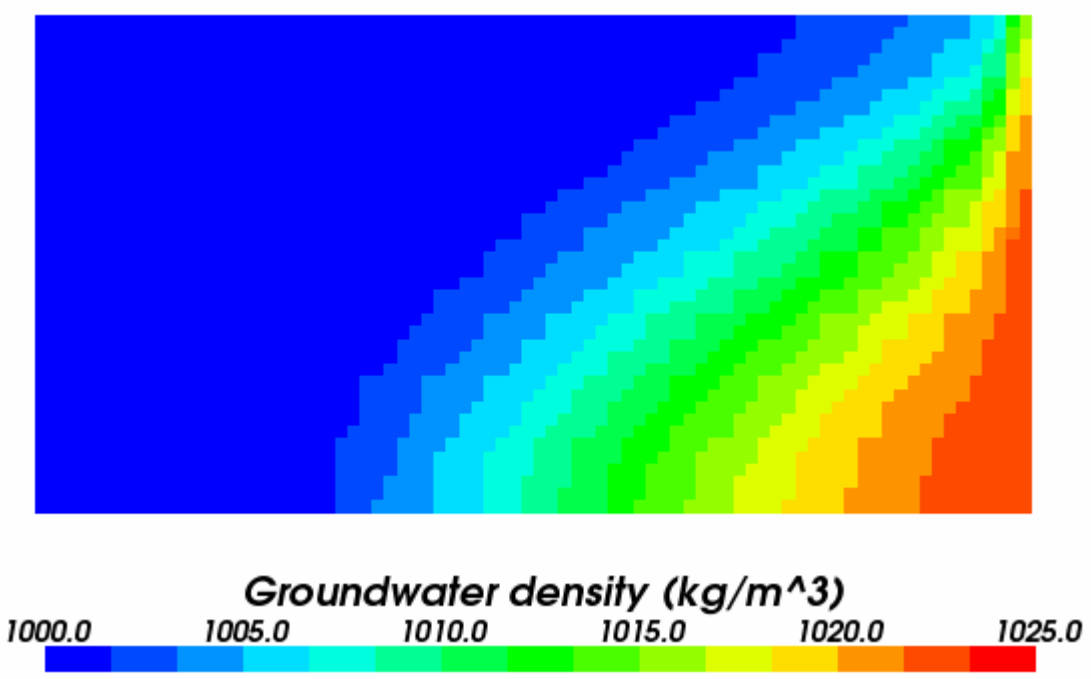

Figure 3-29 Interpolated density

The pressure field is compared against the reference CPM solution. The latter having been separately checked against the analytical solution via the salt concentration.
Plots of the two pressure fields are shown in Figure 3-30 and Figure 3-31. The pressure fields agree to within 5%.

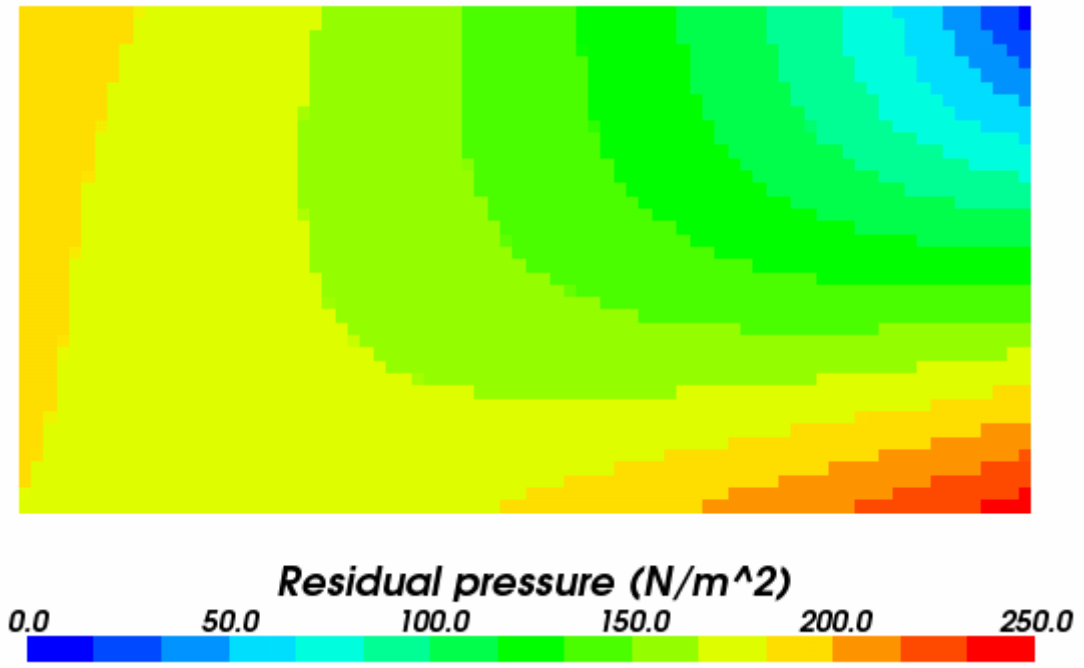

Figure 3-30 DFN residual pressure

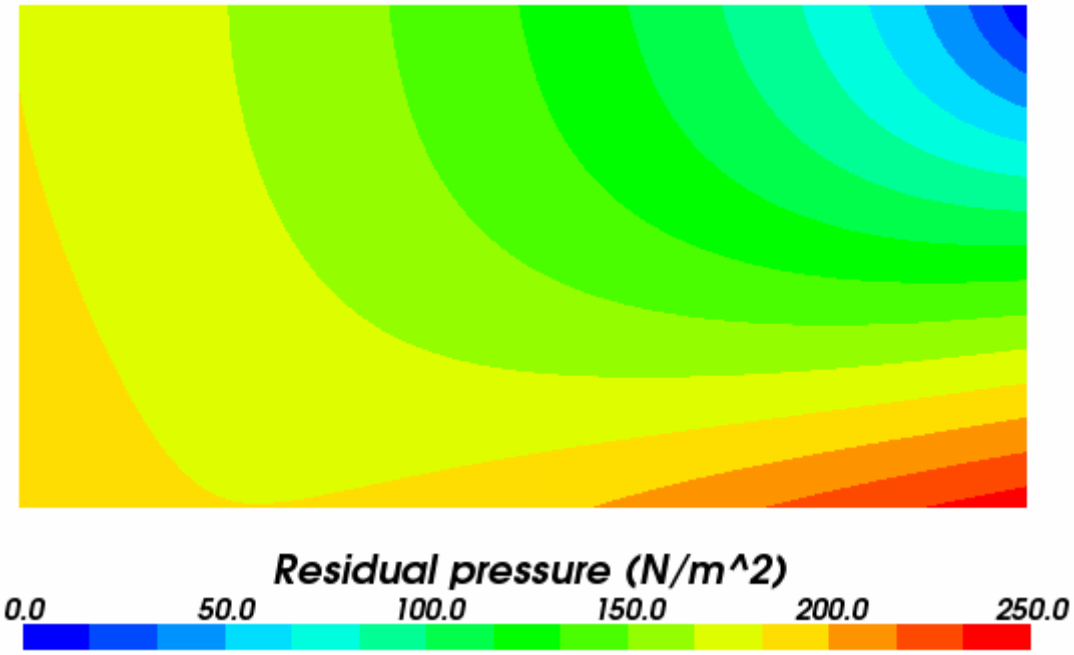

Figure 3-31 Residual pressure CPM

3.8.4.2 Salt Transport

This test case has an analytical solution, represented by an infinite double Fourier series. A truncated form of the series gives a non linear system which can then be iteratively solved. Results from this process are reported in [9] and these are used for comparisons in Figure 3-32. The maximum error in contour location is less than 2%.

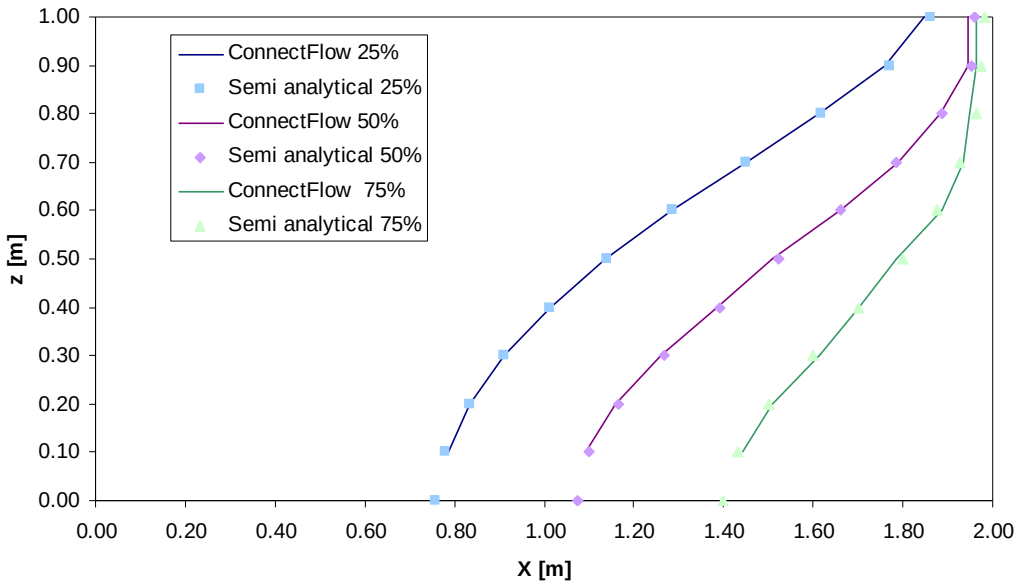

Figure 3-32 Non-dimensional concentration of salinity

4 Combined DFN/CPM Verification

A summary of the DFN/CPM test cases is given in Table 4-1

Case	Title	Overview
4.1	Radial steady state flow.	Steady state groundwater flow with a borehole used to apply the required mass flow boundary condition. The DFN/CPM interface is modelled using the Mass Lumped and Linearly Distributed options. Truncated variations of the domain are used to test current value boundary conditions in the DFN and CPM part of the model.
4.2	2D steady state flow	Steady state groundwater flow from a CPM region with anisotropic permeability to a DFN region.
4.3	2D steady state flow with particle tracks.	Particle tracking through steady state groundwater flow with varying permeability.

Table 4-1 DFN/CPM verification tests

4.1 Radial Steady State Flow

4.1.1 Overview

This case models steady groundwater flow in a 2D disk where water is removed from the centre at a constant rate and the outer disk boundary is maintained at a constant head.

4.1.2 Problem Definition

The problem definition and solution is taken from Feftra [3] and is the DFN/CPM equivalent of case 2.1. The model domain is split up into two regions, fractured rock in the centre of the disk surrounded by porous medium rock, as is illustrated in Figure 4-1. The properties of the fractures and porous medium rock are selected such that the solution is the same as in case 2.1.

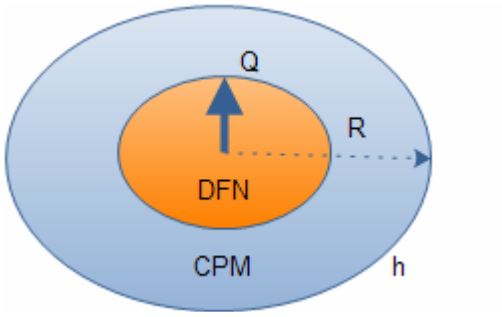

Figure 4-1 Schematic of problem definition

Symbol	Parameter	Value
h	Head at r = R	0 m
Q	Outflow from disk	8.17E-6 m^3/s
K_f	Hydraulic Conductivity Fracture	8.17E-3 m/s
K_r	Hydraulic Conductivity Rock	8.17E-7 m/s
R	Radius of rock	2000 m
e	Aperture of fracture	1.0E-4 m
d	Thickness of disk	1 m
r	Radial distance from axis	0-2000 m
ρ	Density	1000 kg/m^3
μ	Viscosity	1.0E-3 Pa.s
g	Gravity	9.8 m/s^2

Table 4-2 Input parameters

The product of the hydraulic conductivities and thickness are chosen to be constant across the domain, with the hydraulic conductivity of the fracture being derived from the fracture aperture as follows.

$$K_f = \frac{\rho g e^2}{12\mu}$$

The outflow rate is then set to make the solution the same as in 2.1.5.

4.1.3 Variations

The modelled domain consists of a 15 degree sector. The region r<1000 m is modelled as a planar tessellated fracture using the DFN model. The region 1000<r<2000 m is modelled as rock using the CPM model. The fractures and mesh are shown in Figure 4-2.

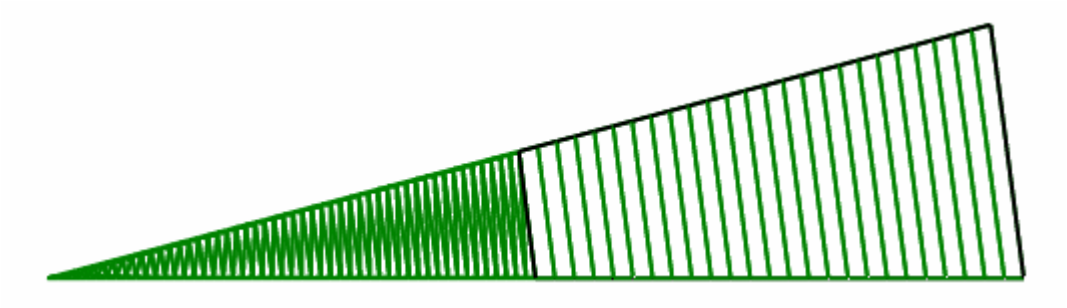

Figure 4-2 Fractures and CPM Mesh

4.1.3.1 Mass lumped ConnectFlow Fluxes

The interface between the two regions is modelled using the interface options, `CONSERVE FRACTURE FLUX` and `MASS LUMP NAPSAC FLUXES`.

4.1.3.2 Current Value in CPM Region

In this variant, the modelled domain is truncated at a radius of 1500 m, and the interpolated solution from the CPM case 2.1.3.1 is applied as a pressure boundary condition. The `MASS LUMP NAPSAC FLUXES` interface option is used.

4.1.3.3 Current Value in DFN Region

In this variant, the modelled domain is truncated at a radius of 250 m, and the interpolated solution from the CPM case 2.1.3.1 is applied as a pressure boundary condition. The `MASS LUMP NAPSAC FLUXES` interface option is used.

4.1.3.4 Linearly Distributed ConnectFlow Fluxes

The interface between the two regions is modelled using the default interface options, `CONSERVE FRACTURE FLUX` and `LINEARLY DISTRIBUTE NAPSAC FLUXES`.

4.1.4 Results

The analytical solution is given by

$$h(r) = h(R) - \frac{Q}{2\pi Kd}\ln(\frac{R}{r})$$

The results from DFN/CPM calculation show good overall agreement with the analytical solution, as illustrated in Figure 4-3 to Figure 4-6. The mass lumping method is more computationally efficient, but the linear distributed fluxes method gives a smoother and more accurate solution.

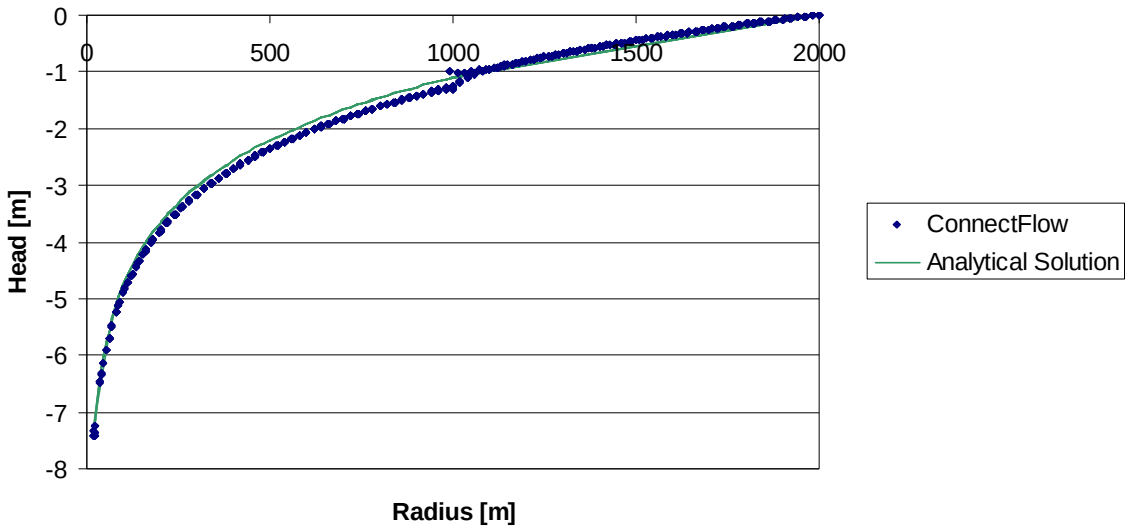

Figure 4-3 Variation of head with distance using a mass lumped DFN/CPM interface

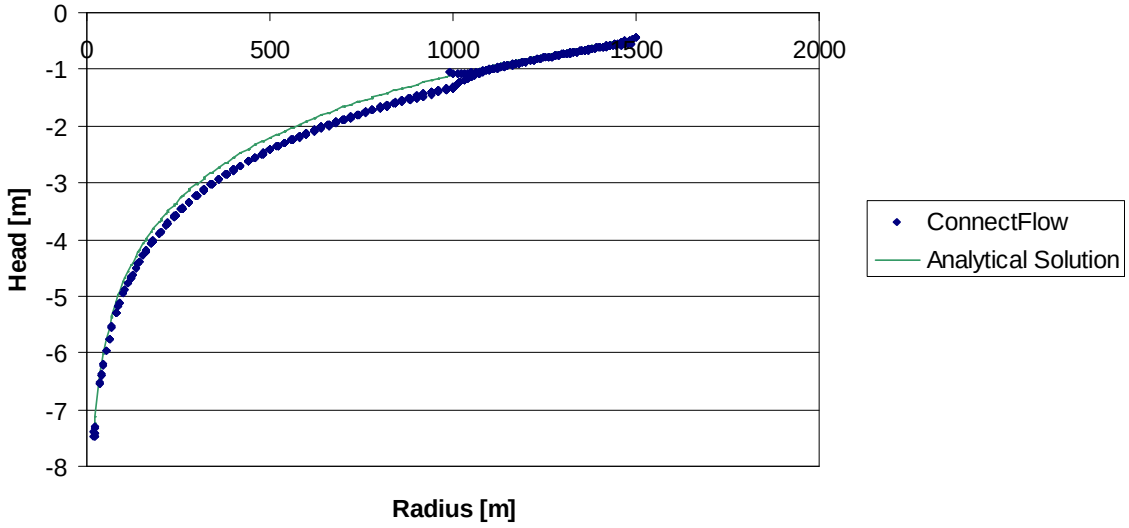

Figure 4-4 Variation of head with distance using a current value boundary in the CPM region and a mass lumped DFN/CPM interface

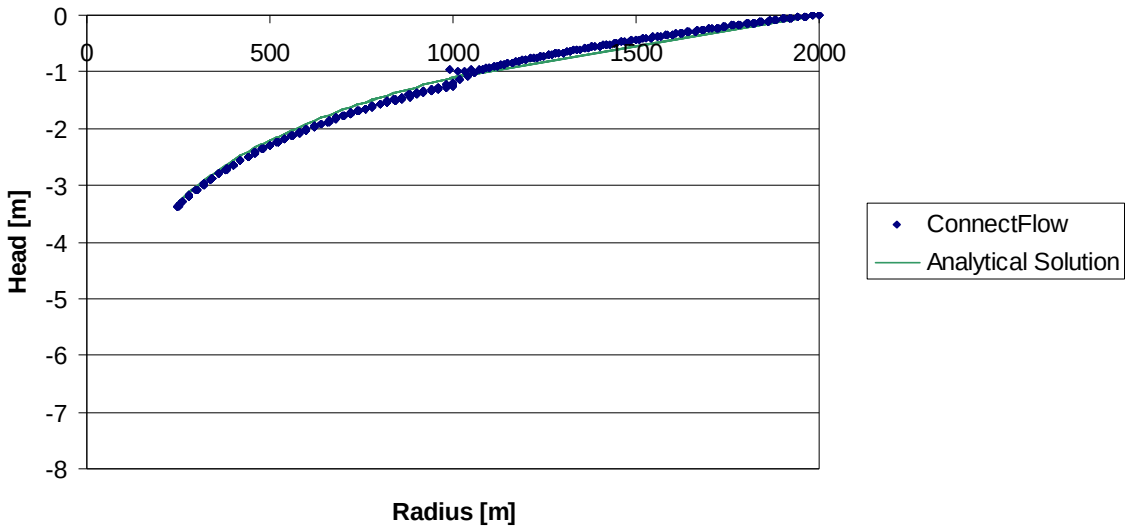

Figure 4-5 Variation of head with distance using a current value boundary in the DFN region and a mass lumped DFN/CPM interface

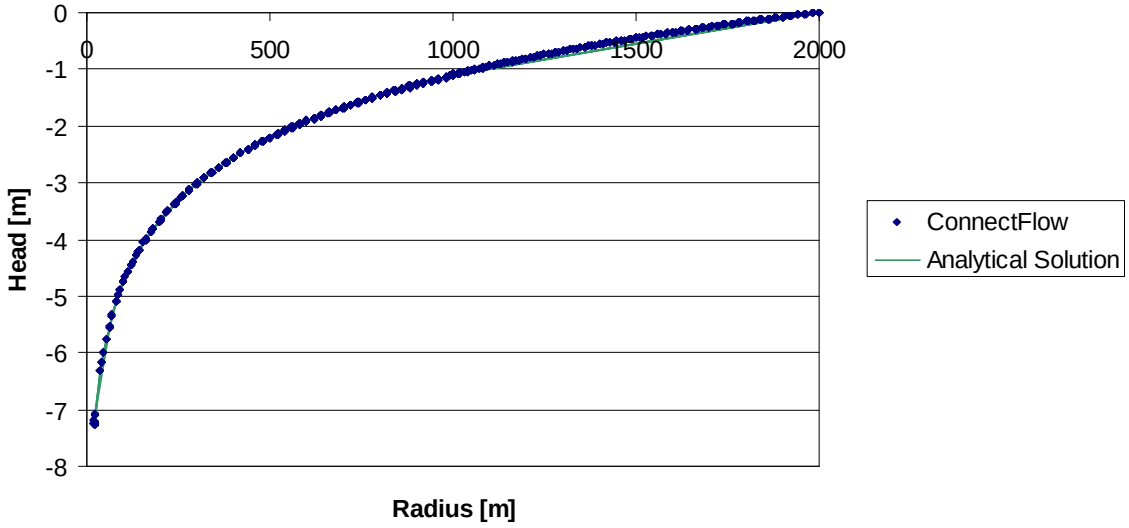

Figure 4-6 Variation of head with distance using a linearly distributed DFN/CPM interface

4.2 Flow to Fracture Network

4.2.1 Overview

This case models steady state groundwater flow in a simple two-dimensional fracture network where the flow enters the network through porous medium rock with anisotropic permeability.

4.2.2 Problem Definition

The problem is a variant of test 3.6, as illustrated in Figure 4-7.

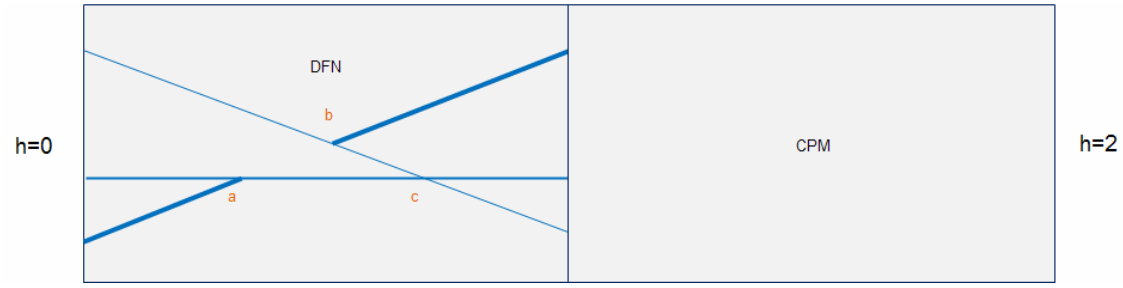

Figure 4-7 Schematic of problem definition

The fracture properties are the same as in Section 3.6.3.2.

The CPM properties are defined in such a way as to ensure the following conditions at the interface.

$$h_{DFN} = h_{CPM} = 1 \text{ m}$$

$$Q_{DFN} = Q_{CPM} = KA\nabla h$$

Where K is the hydraulic conductivity and A the cross sectional area of the CPM region.

The first equation defines the head gradient in the CPM region, and the second is then used in conjunction with the DFN analytical value of Q to obtain K.

As the flow needs to enter the DFN region through the three fractures, there will also be a vertical component to the flow in the CPM region. In order to avoid this impacting the head at the fracture inflows the vertical component or permeability is set to be 1000 times higher than the horizontal component.

4.2.3 Results

The calculated heads are all within 4% of the analytical solution.

Intersection	ConnectFlow	Analytical	% Error
a	0.062	0.061	1.42%
b	0.936	0.968	3.36%
c	0.598	0.600	0.19%

Table 4-3 Heads at fracture intersections

4.3 2D Steady State Flow with Particle Tracks

4.3.1 Overview

This case is taken from Level 3 of the international HYDROCOIN project for verification of groundwater flow codes [22]. It models steady state flow in a two-dimensional vertical slice of rock, containing a circular region of higher permeability.

The case has a non-uniform analytical solution and is used in the HYDROCOIN study to test particle tracking.

This is the equivalent DFN/CPM test of case 2.3.

4.3.2 Problem Definition

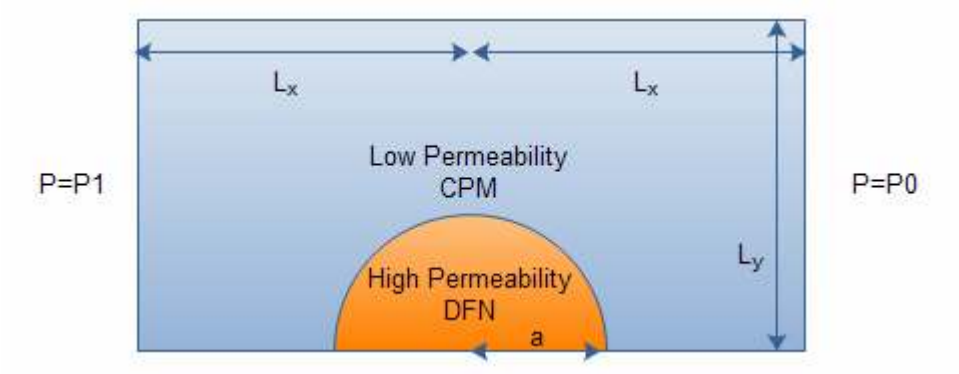

Figure 4-8 Schematic of problem definition

The DFN region is represented by a single tessellated fracture. In order to ensure that the solution is consistent with [22], the following relations must hold.

Balancing the flow rate Q: $k_i d = k_f e$

Fracture permeability: $k_f = \frac{e^2}{12}$

Thickness available for flow: $d = e / \phi$

Taking ϕ from [22], selecting d = 1 m and scaling the pressure gradient gives the values in Table 4-4.

Symbol	Parameter	Value
Lx	Upstream and downstream distances	250 m
Ly	Vertical outer region distance	240 m
a	Radius of inner disk	10 m
P1	Upstream pressure	3.0E-4 Pa
P0	Downstream pressure	-3.0E-4 Pa
k_o	Permeability of outer region	8.333E-7 m^2
k_i	Permeability of inner region	8.333E-5 m^2
k_f	Fracture permeability	8.333E-4 m^2
e	Fracture thickness	0.1 m

d	CPM thickness	1 m
ϕ	Porosity	0.1
ϕ_f	Fracture Porosity	1.0
ρ	Density	1000 kg/m^3
μ	Viscosity	1.0E-3 Pa.s

Table 4-4 Input parameters

Eight particle tracks are released 50 m upstream of the disk centre and at Y values of 10, 12, 14, 16, 18, 20, 22 and 24 m.

The analytical solution for the pathlines is given in the HYDROCOIN report [7] as

$$y = y_o / (1 + \frac{a^2}{r^2} \frac{(k_i - k_o)}{(k_i + k_o)}) \quad \text{for r > a}$$

$$y = y_o \frac{(k_i + k_o)}{2k_o} \quad \text{for r < a}$$

Where r is the distance from the centre of the disk and y_0 is a constant representing the height of the track a long distance away from the origin.

4.3.3 Variations

4.3.3.1 Regular Particle Tracking

Regular particle tracking was used within the CPM region. The mesh around the DFN region is shown in Figure 4-9.

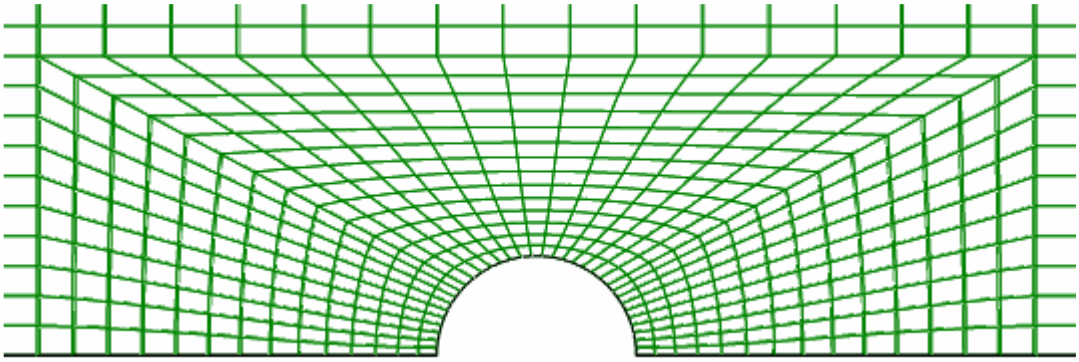

Figure 4-9 CPM wrapped mesh

The tessellated fractures within the inner region are shown in Figure 4-10.

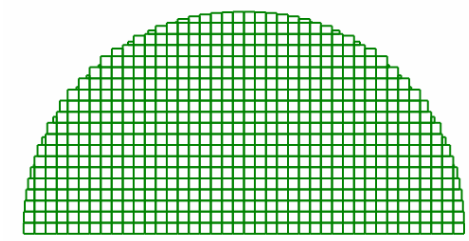

Figure 4-10 Tessellated fractures (larger scale image).

4.3.3.2 Mass Conserving Particle Tracking

Mass conserving particle tracking was used within the CPM region. The mesh around the DFN region is shown in Figure 4-11.

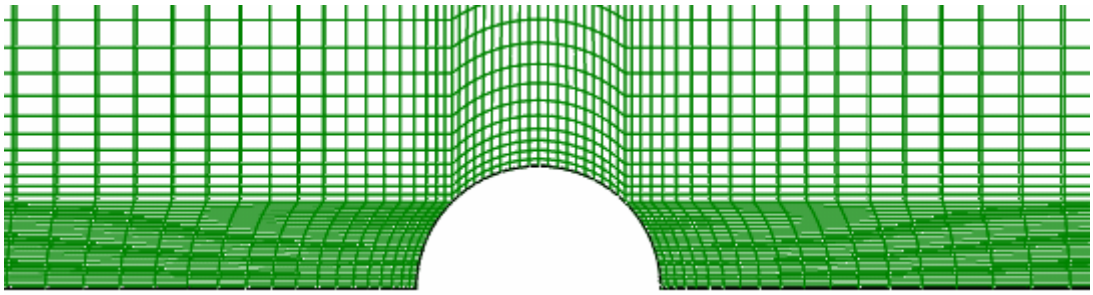

Figure 4-11 CPM regular mesh

The tessellated fractures within the inner region are shown in Figure 4-12.

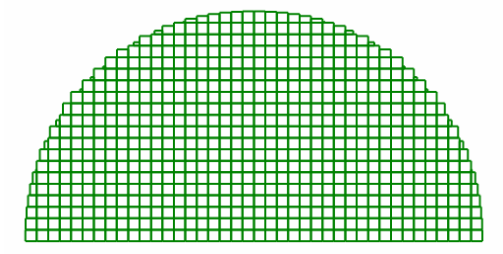

Figure 4-12 Tessellated fractures (larger scale image).

4.3.4 Results

The particle tracks within the DFN part of the model are treated in a stochastic manner, allowing different tracks to take different paths. Ten particles were released from each of the starting positions and the results for regular particle tracking are shown in Figure 4-13 and Figure 4-14.

For the tracks that do not pass through the DFN region, the results are within 1% of the analytical solution for the regular particle tracking, and within 2% of the analytical solution for the mass conserving particle tracking.

The stochastic tracks have more variation as expected, however the average tracks starting from each position also have a travel time and final location within 1% of the analytical solution for the regular particle tracks and within 2% of the analytical solution for the mass conserving particle tracking.

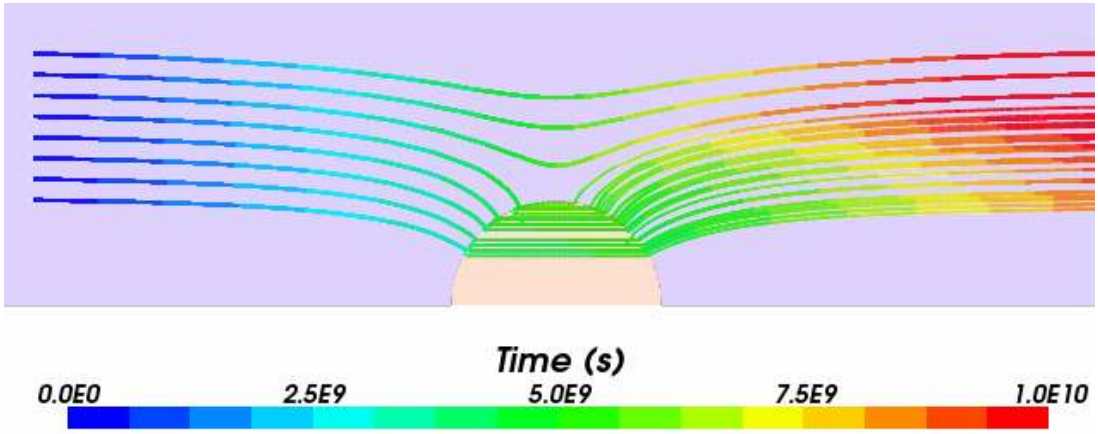

Figure 4-13 Regular particle tracks

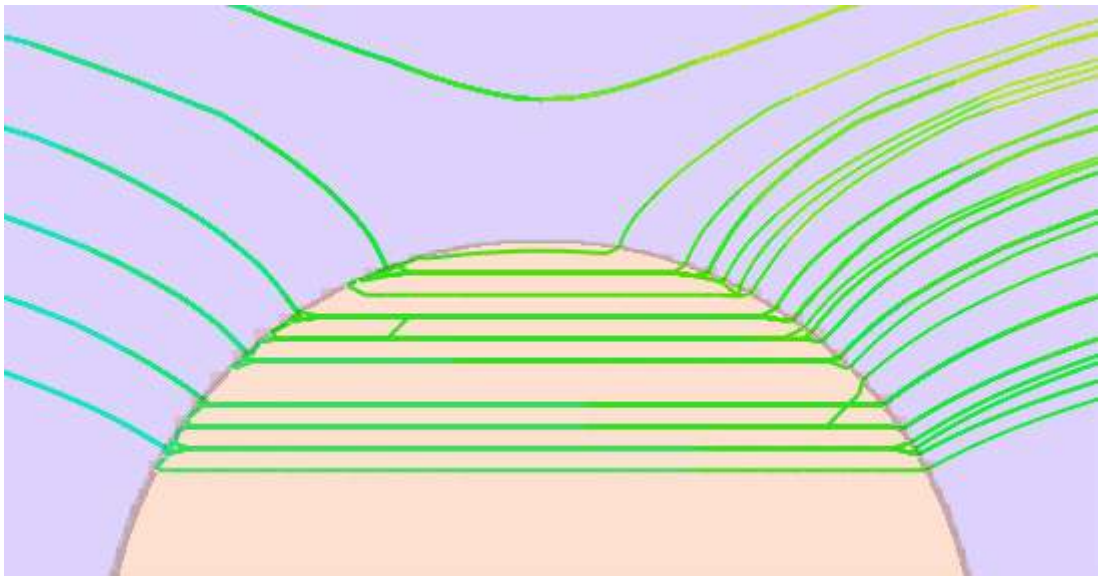

Figure 4-14 Stochastic behaviour of particle tracks

5 Further Testing

This section references further testing that has taken place on the ConnectFlow suite of software, which complements and extends the testing covered in the earlier sections.

5.1 Continuum Porous Media

5.1.1 Verification

5.1.1.1 SKB – Implicit Representation of Fractures

Section 3.3 of SKB report R-01-49 [23] describes the modelling of a set of fractures within a background rock matrix by modifying CPM permeabilties. The approach is tested on a simple 3D case with a semi-analytical solution. The results are all within 20% of the expected solution, with the accuracy improving for larger features. The algorithm allows small features to be modelled more accurately but with increased computational cost.

5.1.1.2 SKB – Heat Transport

Appendix F of SKB report R-06-98 [24] describes three verification tests on heat transport in ConnectFlow. The first case models 1D heat conduction with a time-varying temperature boundary condition. The second case models 1D heat conduction with a specified heat flux boundary condition. The final case models the HYDROCOIN Level 1 Test Case 5 for transient thermal convection in a saturated permeable medium containing a heat source with decaying power output. The first two cases have an analytical solution and the third a semi-analytical solution. In all cases ConnectFlow shows excellent agreement with the expected solutions.

5.1.1.3 SKB R-09-24

Appendix G of SKB report R-09-24 [25] describes a comparison of DarcyTools and ConnectFlow in modelling the inflow of fresh water into a repository under open repository conditions. The ConnectFlow simulation modeled the repository region as a combined DFN/CPM, with boundary conditions being applied from a separate DFN site scale model. DarcyTools used a single regional-scale ECPM model with fine grid refinement around the tunnels. Both models used the same Hydro-DFN data. The overall inflow to the repository agreed to within 20%.

5.1.1.4 ANDRA

A verification exercise for ConnectFlow has been performed for ANDRA [26]. Cases covering a range of groundwater flow and radionuclide transport problems were investigated. The exercise included cases that were diffusion dominated, cases that were advection and dispersion dominated, cases in two- and three-dimensions, and cases with permeability contrasts between regions of the models such that the dominant flow and transport processes differed between the regions. With appropriate choices of the grid, the initial and boundary conditions, and the time-stepping scheme, ConnectFlow was found to accurately reproduce the analytical solutions given for all cases considered.

5.1.1.5 KBS-3

ConnectFlow has also been used in two reviews of repository assessments. These reviews compared the results obtained using different programs for the same finite-element model. In a review of the Swedish KBS-3 study [27], the groundwater heads obtained using ConnectFlow were compared with those obtained using the program GWHRT, for several different cases. In every case, the results agreed to at least six significant figures (the number of figures listed for the output from GWHRT). This gives great confidence that both programs were coded correctly.

5.1.1.6 Gewähr

Results obtained using ConnectFlow were also compared with results obtained using the FEM301 program for the Swiss Project Gewähr [28]. Initially, the results obtained using ConnectFlow differed slightly from those obtained using FEM301. These differences were traced to discrepancies between the FEM301 program and its documentation, and differences between ConnectFlow and FEM301 in the treatment of highly distorted elements. When an appropriate temporary modification was made to ConnectFlow to enable it to mimic the behaviour of FEM301, the results obtained agreed to within five significant figures with those obtained from FEM301. It should be stressed that the initial differences were not due to any problems with ConnectFlow.

5.1.1.7 Nirex

The results of a Monte-Carlo study of dispersion in a heterogeneous porous medium [29] provides a useful and quite stringent test of the groundwater flow and particle transport algorithms used in ConnectFlow. The fact that good agreement could be obtained between the analytical and numerical results for the dispersion of the particles indicates that ConnectFlow provided an accurate solution for the groundwater flow in a heterogeneous permeability field. This case therefore also builds confidence in the correctness of ConnectFlow.

5.1.1.8 Olkiluoto Site

A site scale comparison of FEFTRA and ConnectFlow was carried out as part of the FEFTRA verification [3]. The study showed good agreement with regard to borehole pressures and flow rates near the repository. Flow path positions near the repository were also in good agreement although the travel times were shorter in FEFTRA as compared with ConnectFlow.

A further study [30] has compared modelling of pressures and salinity distributions in 15 deep core drilled boreholes between the codes and measurements based on simulations of the evolution of coupled groundwater flow and solute transport over the last 8000 years.

5.2 Discrete Fracture Network

5.2.1 Verification

5.2.1.1 Stripa

This testing exercise formed part of an OECD/NEA [31] project relating to the final disposal of highly radioactive waste in crystalline rock, that involved a detailed characterisation of the granite formation in an abandoned iron ore mine at Stripa in central Sweden.

The testing compared fracture generation, steady state flow and particle tracking for the fracture flow codes ConnectFlow, FracMan/MAFIC and FMG.

Eight test cases were considered and the ConnectFlow results compared well with available analytical solutions and the results of FracMan/MAFIC and FMG (when a formulation of the test case was possible).

5.2.1.2 Nirex

This study [32] compared transient flow for the fracture flow codes ConnectFlow and FracMan/MAFIC for six test cases. ConnectFlow and FracMan/MAFIC gave qualitatively similar results. However, significant quantitative differences were observed even for quite simple test networks. These are thought to be due to inadequate mesh discretisation of the source zone in FracMan/MAFIC. The ConnectFlow results for the early time behaviour compared well with the available analytical solutions, whereas FracMan/MAFIC gave source zone responses that were inaccurate. The asymptotic ConnectFlow results were shown to tend to the steady state solutions.

5.3 Automated Testing

The test cases presented in this document can be automatically re-run to check the results against the analytical and benchmark data.

This complements the regular ConnectFlow regression test suite, which consists of more than 200 tests and is used to comprehensively check results from new releases of the software against previous versions.

5.4 Peer Review

ConnectFlow is used by a wide variety of organisations with an interest in radioactive waste disposal. There are representatives of both the regulatory bodies and the nuclear utilities. Many of these participate in the iConnect club and provide valuable feedback that helps enhance the software quality.

6 References

1 NAMMU Technical Summary, SA/ENV/CONNECTFLOW/8 August 2008
2 NAPSAC Technical Summary, SA/ENV/CONNECTFLOW/12 , August 2008
3 FEFTRA Verification, VTT Research Notes 2385, Espoo 2007.
4 de Marsily, G., 1986. Quantitative Hydrogeology – Groundwater Hydrology for Engineers. Academic Press INC, Orlando.
5 NEA/SKI, The International HYDROCOIN Project, Level 1: code verification,OECD Publications, 1988.
6 R. Atkinson, T.P. Cherill, A.W. Herbert, D.P. Hodgkinson, C.P. Jackson, J. Rae and P.C. Robinson, Review of the groundwater flow and radionuclide transport modelling in KBS-3, UKAEA Report AERE-R. 11140, 1984
7 NEA/SKI, The International HYDROCOIN Project, Level 3: uncertainty and sensitivity analysis ,OECD Publications, 1991.
8 K. Pruess, TOUGH2 – A General Purpose Numerical Simulator for Multiphase Fluid and Heat Flow, Lawrence Berkeley Laboratory Report LBL–29400, 1991.
9 Improving the worthiness of the Henry problem as a benchmark for density dependent ground water flows. Water Resources Research Vol 40, 2004.
10 A R Hoch, C P Jackson Rock-matrix diffusion in transport of salinity. SKB Report R-04-78.
11 C. M. Oldenburg and K. Pruess. EOS7R: Radionuclide Transport for Tough2, Lawrence Berkley Laboratory Report LBL-34868, Berkley, CA, November 1995.
12 Javandel, I., C. Doughty, and C.-F. Tsang, Groundwater Transport, Handbook of Mathematical Models, American Geophys. Union, pp. 14-19, 1984.
13 Hall, P. (1982). "On Some Simple Estimates of an Exponent of Regular Variation". Journal of the Royal Statistical Society*, Series B (Methodological)* 44 (1): 37–42.
14 A. Banerjee, I. S. Dhillon, J. Ghosh, and S. Sra. Clustering on the Unit Hypersphere using von Mises-Fisher Distributions. JMLR, 6:1345–1382, Sep 2005.
15 Aitchison, J. and Brown, J.A.C. (1957) *The Lognormal Distribution*, Cambridge University Press.
16 Robinson P.C. 1984, Numerical calculations of critical densities for lines and planes. J.Phys. A:Math. Gen. 17, 2823-2830.
17 Bour and Davey 1998, On the connectivity of three dimensional fault networks, Water Resources Research, Vol 34
18 DECOVALEX Task C Stage 1 Project Progress Report, Lanru Jing and John Hudson, 2009
19 DarcyTools, Version 2.1 Verification and validation R-04-21. Urban Svensson, Computer-aided Fluid Engineering AB, Sweden. March 2004
20 NEA/SKI, The International HYDROCOIN Project, Level 1: code verification,OECD Publications, 1988.
21 R. Atkinson, T.P. Cherill, A.W. Herbert, D.P. Hodgkinson, C.P. Jackson, J. Rae and P.C. Robinson, Review of the groundwater flow and radionuclide transport modelling in KBS-3, UKAEA Report AERE-R. 11140, 1984
22 NEA/SKI, The International HYDROCOIN Project, Level 3: uncertainty and sensitivity analysis ,OECD Publications, 1991.
23 Lee Hartley, Peter Jackson, Mike Poole Development of hydrogeological modelling tools based on NAMMU SKB Report R-01-49
24 Lee Hartley, Andrew Hoch, Peter Jackson, Steve Joyce, Rachel McCarthy, William Rodwell, Ben Swift, Groundwater flow and transport modelling during the temperate period for the SR-Can assessment, SKB Report R-06-98.
25 S. Joyce et al, Groundwater flow modelling of periods with temperate climate conditions - Laxemar, 2010.
26 S P Watson, M J Poole and A R Hoch, NAMMU Implementation of Test Cases for Flow and Transport in Porous Media, AEA Technology Report 14302/00/1 Issue 1, 2000.
27 R Atkinson, T P Cherrill, A W Herbert, D P Hodgkinson, C P Jackson, J Rae and P C Robinson, Review of the Groundwater Flow and Radionuclide Transport Modelling in KBS-3, UKAEA Report AERE R.11140, 1984.
28 P C Robinson, C P Jackson, A W Herbert and R Atkinson, Review of the Groundwater Flow Modelling of the Swiss Project Gewähr, UKAEA Report AERE R.11929, 1986

29 S T Morris, J D Porter and C P Jackson, An Investigation of the Accuracy of the Spectral Turning Bands Random Field Generator, Nirex Report NSS/R320, 1997.
30 Lofman J and Meszaros F. Modelling of Groundwater Flow and Solute Transport in Olkiluoto - Update 2011, Posiva Working Report 2011-YY, in prep
31 F. Schwartz and G. Lee. Cross-verification Testing of Fracture Flow and Mass Transport Codes. Technical Report 91-29, Stripa Project, 1991
32. Golders Associates -Transient solver cross code comparison between NAPSAC and FRACMAN/MAFIC . 94524312/21 April 1995.